Quaternary Science Reviews 204 (2019) 17–36

Contents lists available at ScienceDirect

Quaternary Science Reviews

journal homepage: www.elsevier.com/locate/quascirev

Lake sediment records of Holocene hydroclimate and impacts of the Mount Mazama eruption, north-central Washington, USA

Byron A. Steinman [a, *], Daniel B. Nelson [b], Mark B. Abbott [c], Nathan D. Stansell [d], Matthew S. Finkenbinder [e], Bruce P. Finney [f]

[a] Department of Earth and Environmental Sciences and Large Lakes Observatory, University of Minnesota Duluth, Duluth, MN, USA
[b] University of Basel, Department of Environmental Sciences – Botany, Schönbeinstrasse 6, 4056, Basel, Switzerland
[c] Department of Geology and Environmental Science, University of Pittsburgh, Pittsburgh, PA, USA
[d] Department of Geology and Environmental Geosciences, Northern Illinois University, De Kalb, IL, USA
[e] Department of Environmental Engineering and Earth Sciences, Wilkes University, Wilkes-Barre, Pennsylvania, USA
[f] Department of Geosciences and Department of Biological Sciences, Idaho State University, Pocatello, ID, USA

ARTICLE INFO

Article history:
Received 9 March 2018
Received in revised form
23 July 2018
Accepted 12 September 2018
Available online 29 November 2018

ABSTRACT

Multi-proxy sediment records from Castor Lake and Scanlon Lake, north-central Washington, provide a late Quaternary perspective on lake/catchment hydrologic and ecosystem responses to climate change and the Mazama volcanic ashfall event. Analyses of authigenic carbonate mineral oxygen and carbon isotope values, organic carbon and nitrogen content, and sedimentological facies were conducted on sediment from Castor Lake in order to reconstruct lake/catchment hydrologic balance, the source and abundance of organic matter, and variations in lake level. Sedimentary facies characterization was conducted on the Scanlon Lake sediment in order to provide supporting evidence for the lake-level shifts inferred from the Castor Lake data. Marked changes in Castor Lake proxy values occur from 12,860 to 11,440 calendar years before present (yr BP), suggesting lake/catchment responses to the Younger Dryas cold reversal including higher lake levels, substantial variability in productivity, and increased catchment erosion. High $\delta^{18}O$ values at 9630 yr BP indicate that lake levels were lower than at present and that the early Holocene was dry. Sedimentological analyses and $\delta^{18}O$ data demonstrate that subsequent to the Mazama climactic eruption (~7600 yr BP), a transition to the lowest lake levels of the Holocene occurred over several centuries, with maximum $\delta^{18}O$ values at 7290 (90% uncertainty range: 7020–7500) yr BP and low lake levels persisting until 6190 (5960–6410) yr BP. Lithological changes in the Scanlon Lake record support these inferences. The lowest $\delta^{18}O$ values of the Holocene occur in sediment from ~5000 yr BP, indicating high lake levels at this time, after which a secular trend toward higher $\delta^{18}O$ values and lower lake levels occurred. The prolonged lowstand in the centuries following the Mazama eruption suggests that catchment hydrologic characteristics were strongly impacted by the ashfall through effects on soil water retention capacity, that similar responses may have occurred in comparable settings within the Mazama ashfall zone, and that such volcanic events have the potential confound the climate signal in lake sediment records. Were a similar event to happen in the future, catchment hydrology, stream/river discharge, and lake/catchment ecosystem dynamics could be affected for centuries.

1. Introduction

Lake sediments can provide a wealth of information on past changes in both terrestrial and lacustrine environments over timescales ranging from years to millennia. In North American landscapes that formed after the Last Glacial Maximum, lakes are ubiquitous and provide a wide spatial distribution of geologic archives from which paleoenvironmental records can be developed. Such records provide much of the basis of our understanding of late Quaternary climate change in middle/high latitude continental interiors and are complementary to other paleoclimatological and paleoceanographic archives such as tree rings, ice cores, ocean sediments and corals. Here, we apply a multi-proxy approach to the analysis of sediment from Castor Lake, north-central Washington,

* Corresponding author.
E-mail address: bsteinma@d.umn.edu (B.A. Steinman).

https://doi.org/10.1016/j.quascirev.2018.09.018
0277-3791/

that provides information on variations in catchment vegetation, lake productivity, lake/catchment hydrology, and the climatic and volcanic forcing factors likely responsible for these changes since the retreat of the Cordilleran ice sheet from this region ~14,000 calendar years before present (yr BP) (CE, 1950) (Clague and James, 2002). We also present results of analyses of sediment from Scanlon Lake, located adjacent to Castor Lake, that offer information on changes in lake level during the middle Holocene.

The overall objective of this research is to provide a millennial timescale context for understanding the modern mean state and variability of climate in the generally dry, drought-prone, Columbia River watershed of Washington. The climate east of the Cascade Mountains is largely semi-arid with a long, warm, and dry growing season that supports irrigation-based agriculture. As such, the economy of the interior Pacific Northwest is largely reliant on cold season precipitation and snowmelt derived runoff to recharge groundwater aquifers and maintain river flow during the warm season (Barnett et al., 2004; Mote et al., 2003; Stewart et al., 2005). Castor Lake and Scanlon Lake are adjacent to the Okanogan River, a major tributary of the Columbia River, and are therefore well positioned to archive information on past changes in the hydroclimate and hydrologic balance of this drought sensitive region (Fig. 1).

Analyses of the stratigraphy and organic and geochemical constituents of lake sediment can reveal a great deal about the influence of climate variability on lake/catchment hydrological and biological systems (e.g. Abbott et al., 2000; Finney et al., 2012; Valero-Garcés et al., 1997). In lakes similar to Castor, that is, with sufficiently high sedimentation rates, low energy depositional environments, and water column chemistry and mixing regimes that promote laminated sediment preservation, records with subdecadal resolution can be developed that are useful for high resolution spatiotemporal climate/environmental investigations (e.g. Abbott et al., 1997; Jones et al., 2006; Roberts et al., 2001). Surficially closed-basin lakes (that lack substantial groundwater throughflow), in particular, are sensitive to changes in the catchment hydrologic balance on seasonal or longer timescales and can provide records of past lake-level change in response to variations in hydroclimate (Kirby et al., 2012; Shuman et al., 2010; Stone and Fritz, 2006). Assessment of sedimentary facies (e.g. the presence and/or absence of laminae) and sedimentology (e.g. carbonate, organic, and residual minerogenic content) can inform on a variety of factors including past changes in stratification, catchment weathering, and lake level (e.g. Shuman et al., 2001; Stansell et al., 2010; Valero-Garcés and Kelts, 1995). A highly informative

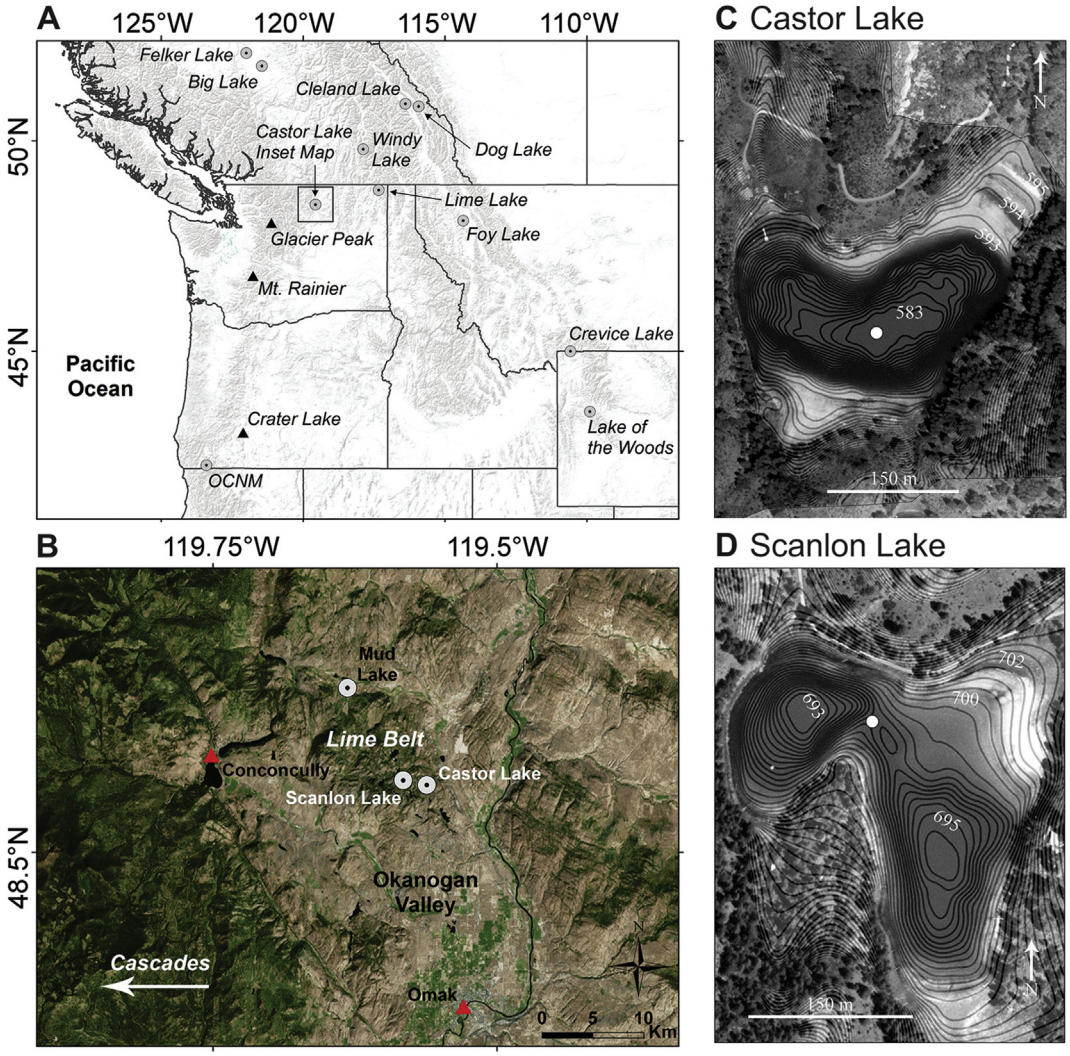

Fig. 1. (A) Map of the greater Pacific Northwest region depicting the location of Castor Lake, Scanlon Lake, and other study sites. (B) Inset map of the Lime Belt region of north-central WA. Scanlon Lake is located 1.2 km to the west and ~90 m above Castor Lake. Bathymetric map of (C) Castor Lake and (D) Scanlon Lake with coring locations indicated by filled white circles.

paleoproxy, the oxygen and carbon isotopic composition of lacustrine carbonate minerals (i.e. calcite/aragonite $\delta^{13}C$ and $\delta^{18}O$) can provide insight on past variations in lake/catchment hydrologic balance, depending the on the hydrologic characteristics of the study lake (Anderson et al., 2016; Jones and Roberts, 2008; Stansell et al., 2013). Complementary assessment of the concentration of organic components of the sediment (% C, % N, C/N) can inform on variations in primary productivity, the influx of terrestrially derived organic matter, and the provenance (either aquatic or terrestrial) of organic matter deposited in lake basins (Finkenbinder et al., 2014; Finney et al., 2000; Talbot and Johannessen, 1992).

We applied each of these analytical methods to sediment cores collected from Castor Lake, north-central Washington, and assessed the lithostratigraphy of sediment cores from nearby Scanlon Lake, using ^{210}Pb, ^{137}Cs, ^{14}C and tephrochronology dating techniques to provide chronological constraint for both records. Our interpretations are based on generally accepted paleolimnological proxy models (e.g. Leng and Marshall, 2004; Li and Ku, 1997; Talbot, 1990) and site specific lake/catchment modeling studies (Steinman et al., 2010a, 2010b), as well as reviews of other paleoclimate records from the greater Pacific Northwest region (Hebda, 1995; Steinman et al., 2016; Whitlock, 1992). This manuscript builds upon the work of Nelson et al. (2011) by extending the Castor Lake $\delta^{18}O$ record from 6000 yr BP through the Younger Dryas, focusing on potential impacts of the Mazama climactic eruption and ashfall on lake/catchment hydrologic balance, and providing insight on the timing and relationships between inferred early and middle Holocene lake lowstands and externally forced changes in hydroclimate.

2. Study area

Castor Lake (48.5394° N, 119.5615° W; 601 m amsl) (Fig. 1) is a small (surface area ~0.062 km^2) predominantly closed-basin, alkaline (450–575 mg/L as $CaCO_3$) system with a water residence time of ~2.5 years (Steinman et al., 2010b). Maximum water depth averages ~11 m and has been observed (directly and via aerial/satellite imagery) to vary both seasonally and interannually up to ~3 m in response to changes in precipitation and evaporation rates (Steinman et al., 2013, 2010b; Steinman and Abbott, 2013). Field bathymetry surveys indicate a single large, flat basin with gently sloping littoral shelves on the northeastern, northwestern, and southern sides of the lake. Overflow occurs along the northeastern shoreline during exceptionally wet periods and was observed four times between CE 1950 and 2012 (Steinman et al., 2013) and most recently in 2017/2018. Littoral zone vegetation is minimal and carbonate shelf deposits are visible to a depth of several meters. The Castor Lake catchment (0.858 km^2) is generally steep sided and located on a regional topographic high that is isolated from distal groundwater aquifers, with vegetation consisting of *Artemisia* (sagebrush), *Poaceae/Gramineae* (grasses), and scattered forest of *Pinus* (pine) *ponderosa*. Bedrock geology in the catchment is mapped as the Triassic age Cave Mountain Formation, consisting of calcareous slate, limy phyllite, metalimestone, and basalt flows (Rinehart and Fox, 1976). Surficial geology in the catchment is mapped as Pleistocene age glacial drift, consisting of a discontinuous and thin cover of silt, sand, and gravel deposits (Rinehart and Fox, 1976). The warm season (April–September) water column profiles of Castor Lake indicate well-developed stratification. In contrast, cold season (October–March) profiles indicate a lack of stratification (and therefore seasonal vertical mixing) either throughout the water column (in the case of the 10/25/08 profile) or to a depth just above the sediment water interface (Fig. 2). However, anoxia in the hypolimnion was measured in all seasons, indicating that any bottom-water oxygenation that may occur is sporadic. This partially meromictic state in part results from wind sheltering provided by the steep-sided catchment.

Castor Lake alkalinity and pH measurements indicate that the dissolved inorganic carbon (DIC) pool consists primarily of bicarbonate, and water chemistry measurements demonstrate relatively high concentrations of several predominantly conservative ions including Mg^{2+} (20–40 meq/L) and SO_4^{2-} (19–30 meq/L) (Steinman et al., 2013). The high salinity is a result of strong evaporative control on the hydrologic budget, as determined through hydrologic and isotope mass balance modeling experiments and analysis of water isotope values (Fig. 3) (Steinman et al., 2010b). The comparatively lower concentration of Ca^{2+} (0.5–2.2 meq/L) is a result of the precipitation of aragonite from the water column during the spring and summer months in response to inferred biomediated increases in pH, reduction of $CaCO_3$ solubility due to higher water temperatures, and greater concentrations of Ca^{2+} and HCO_3^{2-}/CO_3^{2-} as a consequence of water losses via evaporation (Steinman et al., 2013). The precipitation of aragonite from the Castor Lake water column is therefore Ca^{2+} limited and dependent upon the inflow of catchment derived water (Nelson et al., 2011; Shapley et al., 2005), which has much higher Ca^{2+} concentrations (~4.4–8.6 meq/L) than the lake water (Steinman et al., 2013).

Scanlon Lake (48.5417° N, 119.5818° W; 694 m amsl) (Fig. 1) is located 1.2 km to the west of Castor Lake and shares similar characteristics. The lake has a relatively small surface area (~0.047 km^2), closed-basin hydrology, alkaline water chemistry (485–1130 mg/L as $CaCO_3$), high concentrations of conservative ions including Mg^{2+} (39–186 meq/L) and SO_4^{2-} (45–202 meq/L), and a water residence time of ~2 years (Steinman et al., 2013, 2010b). Surface water $\delta^{18}O$ and δD data and modeling experiments indicate the hydrologic balance of Scanlon Lake is strongly influenced by evaporation, more so than Castor Lake (Fig. 3) (Steinman et al., 2010b). The maximum water depth is ~8 m in the smaller western basin and ~6 m in the larger eastern basin, with substantial changes in lake level occurring seasonally and interannually (Steinman et al., 2010b). The undeveloped, steep sided catchment (0.364 km^2) is isolated from regional groundwater sources, with vegetation consisting principally of *Pinus ponderosa* forest and secondary *Artemisia* and *Poaceae/Gramineae*. The bedrock and surficial geological materials underlying Scanlon Lake are identical to that at Castor Lake, consisting of Triassic age metalimestone and Pleistocene age glacial drift (Rinehart and Fox, 1976). Water column profiles indicate that Scanlon Lake is strongly stratified with an anoxic monimolimnion that is substantially more saline than the surface water (Fig. 4).

The modern climate of north-central Washington is dominated by the Pacific westerlies (Bryson and Hare, 1974). These winds, strongest between 45° and 50°N, are controlled by the strength and position of the Aleutian low-pressure and North Pacific high-pressure systems. During the cold season, the Aleutian Low strengthens and shifts to the south, delivering cool, wet air to Washington. In the warm season, the Aleutian Low weakens, moves northward, and the North Pacific high becomes the predominant climatic control, often blocking the westerly winds and preventing the inland flow of atmospheric moisture from the Pacific. Arctic air masses occasionally enter the region in the cold season, but are generally replaced quickly by westerly derived air from the Pacific basin. Climate normals for the study lakes were determined using data from weather stations located in Conconully (48.5557° N, 119.7492° W; 704 m amsl; NOAA GHCND: USC00451666) and Omak (48.4644° N, 119.5169° W; 396 m amsl; NOAA GHCND: USW00094197) corrected on the basis of correlations with data from a weather station adjacent to Castor Lake (Fig. 5) (Steinman et al., 2013). Mean monthly precipitation $\delta^{18}O$ values vary by as much as ~6‰ throughout the year (waterisotopes.org) (Bowen and Revenaugh, 2003).

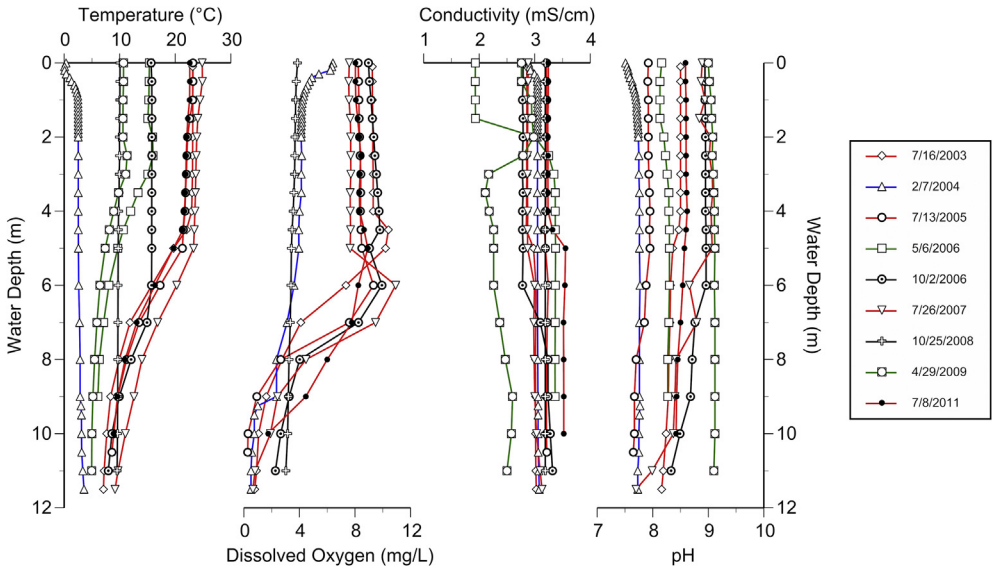

Fig. 2. Castor Lake water column profiles (temperature, dissolved oxygen, conductivity, pH).

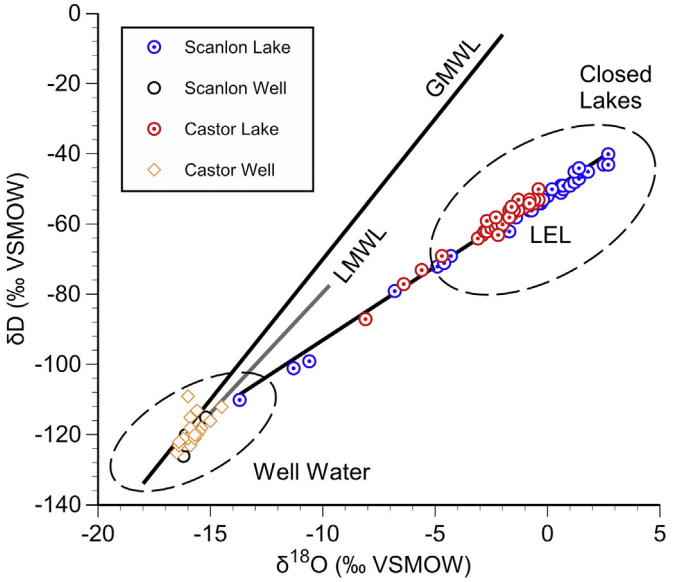

Fig. 3. Water sample isotope data from CE 2003–2015. Well water from the Castor Lake and Scanlon Lake catchments is consistent with both the Global Meteoric Water Line (GMWL) and Local Meteoric Water Line (LMWL). Castor Lake and Scanlon Lake water samples plot along the Local Evaporation Line (LEL). The LEL has a slope of 4.19.

3. Methods

3.1. Water sample collection and analysis

Surface water samples for oxygen and hydrogen isotope analyses were collected from Castor Lake, Scanlon Lake, and wells located in the catchments from CE 2003–2015 (Fig. 3). Water isotope data from CE 2003–2011 were previously reported by Steinman et al. (2013). Water samples were collected in 30 mL high-density polyethylene (HDPE) bottles after rinsing three times with sample water and then filling and capping the bottle underwater. All samples were stored in cool (~4 °C), dark conditions until analysis. Isotopic ratios were measured either at the University of Arizona Environmental Isotope Laboratory on a gas-source isotope ratio mass spectrometer (Finnigan Delta S) or at the Indiana University Purdue University Indianapolis (IUPUI) Department of Earth Sciences on a Picarro L2130-i Analyzer coupled to an autosampler and high-precision water vaporizer unit. At the University of Arizona hydrogen isotope analyses were conducted by reacting samples at 750 °C with Cr metal using a Finnigan H/Device coupled to the mass spectrometer. Oxygen isotope analyses were conducted by equilibrating samples with CO_2 gas at approximately 15 °C in an automated equilibration device coupled to the mass spectrometer. Precision (1σ) was 0.9 per mil (‰) or better for δD and 0.08‰ or better for $\delta^{18}O$ on the basis of repeated measurement of internal standards. At IUPUI water isotope measurements were corrected for memory and drift using calibrated standards from Los Gatos, and precision for δD and $\delta^{18}O$ was 0.6‰ and 0.1‰, respectively. All water isotope results are reported in standard delta notation relative to Vienna Standard Mean Ocean Water (VSMOW). Water column profiles (temperature, dissolved oxygen, conductivity, and pH) were measured using a Hach Hydrolab Water Quality Sonde.

3.2. Sediment core collection

Overlapping Livingstone piston cores (Wright et al., 1984) (five cm diameter) were recovered from Castor Lake during July of 2003 in a water depth of 11.5 m. A 1.25 m percussion core (6.7 cm diameter) of the uppermost sediment was also collected at this time. A freeze core was retrieved from the Livingstone core site in the winter of 2004 using a hollow, steel wedge filled with a dry ice, ethanol slurry. The freeze core preserved an undisturbed sequence of the uppermost sediments. Scanlon Lake sediment samples were collected in July of 2005 using a Livingstone piston corer (five cm diameter) in a water depth of 2.5 m on a littoral shelf (Fig. 1). The Livingstone and percussion cores were wrapped in plastic, placed in polyvinyl chloride (PVC) tubes, and stored at ~4 °C until they were split and sampled at the University of Pittsburgh Department of Geology and Environmental Science. The freeze core was stored in a cooler containing dry ice during shipping and kept frozen prior to sampling. Scanlon Lake surface sediments were transferred to sterile plastic bags in the field at 0.2 cm intervals by upward extrusion into a tray fitted to the top of the core barrel.

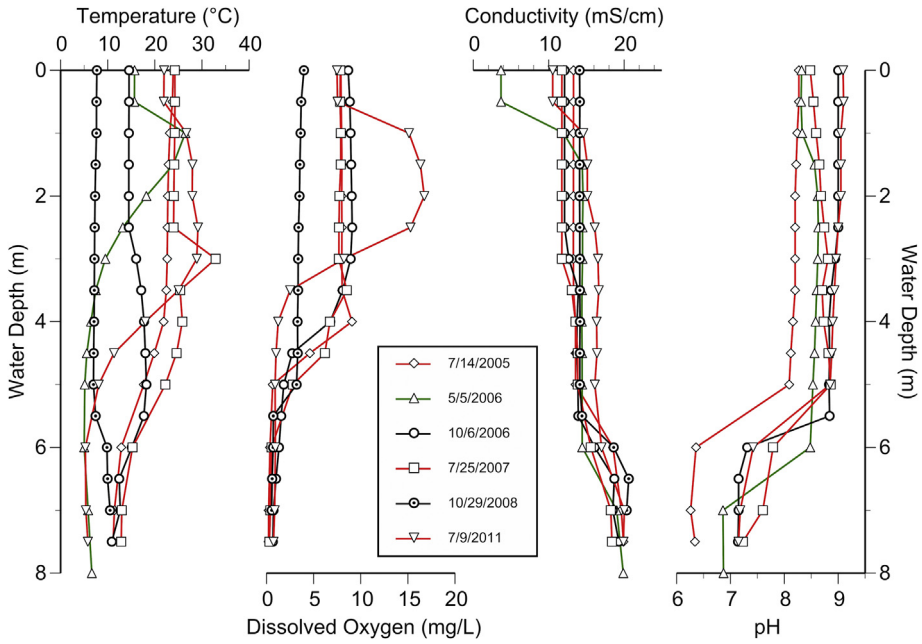

Fig. 4. Scanlon Lake water column profiles (temperature, dissolved oxygen, conductivity, pH).

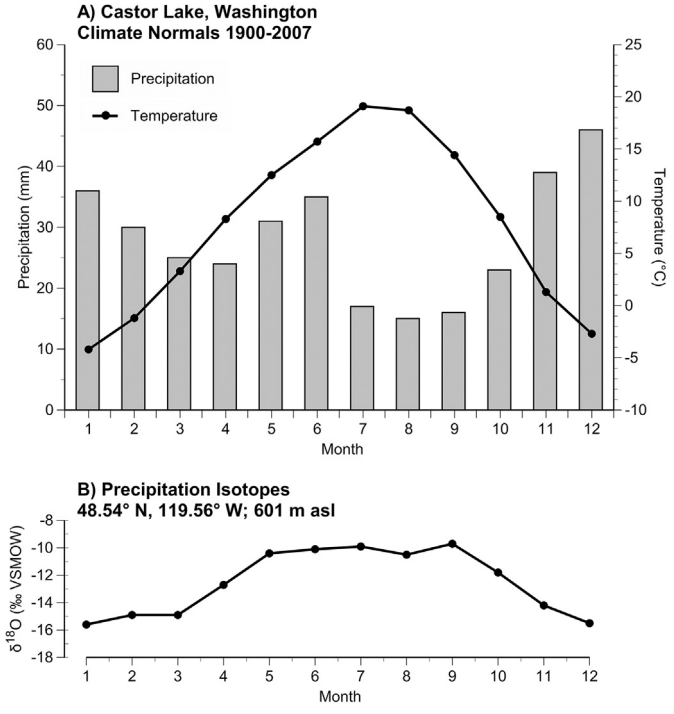

Fig. 5. (A) Average monthly precipitation and temperature data and (B) average monthly precipitation oxygen isotope values for Castor Lake and Scanlon Lake (Bowen and Revenaugh, 2003).

3.3. Sediment core chronology

Chronological control for the Castor Lake sediment record is provided by 11 accelerator mass spectrometry (AMS) radiocarbon dates, two tephras of known age, measurements of ^{137}Cs activity in the surface sediment, and 19 tie-point (tuned) ages based on comparison with tree-ring data (Table 1) (see Steinman et al., 2013 and supplemental information in Nelson et al., 2011). The Scanlon Lake chronology is based on 14 AMS radiocarbon dates, two tephras of known age, and ^{210}Pb measurements (Table 2) (see Steinman et al., 2013 for detail on the ^{210}Pb measurements). Sediment subsamples for radiocarbon dating were disaggregated with 7% H_2O_2 and sieved through a 125-mm screen to isolate identifiable terrestrial macrofossils (charcoal, seeds, and small wood fragments), which were collected using a small brush under a binocular microscope. Radiocarbon analyses of Scanlon Lake samples were conducted at the W.M. Keck Carbon Cycle Accelerator Mass Spectrometry Laboratory at the University of California, Irvine (UCI) after pre-treating at the University of Pittsburgh using a standard acid-base-acid procedure (Abbott and Stafford, 1996). Tephra from the sediment cores were identified via electron microprobe analysis at Washington State University as resulting from either the Mount Saint Helens (MSH) W or Mt. Mazama climactic eruptions. Dendrochronology based estimates date the MSH W tephra to CE 1480 (470 yr BP) (Mullineaux, 1986). The Mt. Mazama climactic eruption dates to either 7627 ± 150 yr BP, as determined by layer counting of the GISP2 ice core (Zdanowicz et al., 1999), or 6730 ± 40 ^{14}C yr BP (7597 yr BP), as determined by radiocarbon dating of lake sediment (Hallett et al., 1997). These ages are in close agreement, and we have applied the radiocarbon-determined age of 6730 ± 40 ^{14}C yr BP in this study.

Composite sediment depth scales were created for each lake based on visual stratigraphic correlation of overlapping cores. Tephra deposits were assumed to be instantaneous events, and their thicknesses were removed from the master depth scale. Bchron, a Baysesian statistical age-model software package for R (Haslett and Parnell, 2008; Parnell et al., 2011, 2008), was used to produce a median age and probability distribution (90% uncertainty range) for each depth increment on the basis of the age control point data, which include the depth interval spanned by the sample, the calibration curve, and the AMS measurement uncertainty. The IntCal13 calibration curve (Reimer, 2013) was applied to estimate radiocarbon age uncertainty, and normal distributions were assumed for uncertainty in the ^{137}Cs and ^{210}Pb control points. The Castor Lake age model presented here is modified from that of Nelson et al. (2011). The differences are that slight adjustments

Table 1
Castor lake chronologic control points.

Total adjusted depth (cm)	^{14}C age (^{14}C yr BP)	1σ uncertainty (yr)	Median age (yr BP)	2σ calibrated age range (yr BP)	Type	Material
0.00	N/A	N/A	−54	N/A	Surface	N/A
5.54	N/A	1	−15	N/A	137Cs	N/A
6.66	N/A	1	−10	N/A	137Cs	N/A
8.33	N/A	1	−5	N/A	137Cs	N/A
20.74	N/A	N/A	144	N/A	tune	N/A
24.82	N/A	N/A	187	N/A	tune	N/A
33.67	N/A	N/A	248	N/A	tune	N/A
40.00	N/A	N/A	335	N/A	tune	N/A
41.00[a]	435	40	495	330–539	14C	Grass
51.74	N/A	N/A	470	N/A	Tephra	Tephra
53.70	N/A	N/A	543	N/A	tune	N/A
57.11	N/A	N/A	613	N/A	tune	N/A
60.70	N/A	N/A	663	N/A	tune	N/A
66.79	N/A	N/A	798	N/A	tune	N/A
67.53	N/A	N/A	839	N/A	tune	N/A
70.65	N/A	N/A	957	N/A	tune	N/A
74.04	N/A	N/A	1010	N/A	tune	N/A
77.22	N/A	N/A	1121	N/A	tune	N/A
81.03	N/A	N/A	1223	N/A	tune	N/A
82.93	N/A	N/A	1250	N/A	tune	N/A
86.11	N/A	N/A	1307	N/A	tune	N/A
89.22	N/A	N/A	1400	N/A	tune	N/A
90.08	N/A	N/A	1424	N/A	tune	N/A
93.77	N/A	N/A	1471	N/A	tune	N/A
93.80[a]	1530	35	1425	1350–1523	14C	Charcoal
118.80	N/A	N/A	1785	N/A	tune	N/A
122.70	1890	35	1837	1725–1917	14C	Pine Needle
188.98	3385	35	3629	3514–3717	14C	Charcoal
214.43	4095	45	4615	4443–4820	14C	Seed
246.40	5160	100	5918	5662–6183	14C	Charcoal
262.42	5815	25	6629	6533–6716	14C	Seed
282.50	6730	40	7597	7514–7666	Tephra	Tephra
306.50[a]	6720	80	7585	7439–7689	14C	Seed
342.50	9425	30	10656	10578–10730	14C	Seed
364.50	10025	35	11515	11330–11710	14C	Seed
388.50	11020	35	12882	12753–13007	14C	Seed

[a] Omitted from Bchron age model.

Table 2
Scanlon lake chronologic control points.

Total adjusted depth (cm)	^{14}C age (^{14}C yr BP)	1σ uncertainty (yr)	Median age (yr BP)	2σ calibrated age range (yr BP)	Type	Material
0	N/A	N/A	−55	N/A	surface	N/A
2.5	N/A	1	−52	N/A	210Pb	N/A
5.5	N/A	1	−38	N/A	210Pb	N/A
8.5	N/A	2	−25	N/A	210Pb	N/A
11.5	N/A	3	−10	N/A	210Pb	N/A
14.5	N/A	5	9	N/A	210Pb	N/A
17.5	N/A	6	21	N/A	210Pb	N/A
20.3	N/A	10	36	N/A	210Pb	N/A
22.1	N/A	14	48	N/A	210Pb	N/A
24	135	15	128	11–271	14C	Bark
37.5[a]	230	15	288	1–303	14C	Pine Needle
53.1	155	15	190	4–281	14C	Wood
71.5[a]	685	50	644	551–695	14C	Charcoal
89.5	365	20	440	319–497	14C	Plant Matter
92	N/A	N/A	470	N/A	Tephra	Tephra
103	610	15	602	551–651	14C	Bark
109.5	925	15	856	793–911	14C	Plant Matter
246.5	3715	15	4032	3985–4143	14C	Bark
279.5	4380	15	4925	4869–5029	14C	Plant Matter
384	6080	25	6941	6860–7138	14C	Plant Matter
400	6240	80	7149	6935–7406	14C	Charcoal
452.5	6400	170	7300	6903–7591	14C	Charcoal
477.5	6730	40	7597	7514–7666	Tephra	Tephra
557	8180	25	9110	9025–9253	14C	Wood
620	10160	20	11860	11724–12008	14C	Wood

[a] Omitted from Bchron age model.

were applied to several of the control point depths on the basis of reassessment of sample locations in the core, and the chronology has been extended from 6000 yr BP to the late Pleistocene.

3.4. Sediment core processing and sampling

Sediment facies for each core sequence were characterized on the basis of visual inspection and loss-on-ignition (LOI) analysis (described below). The Castor lake core sequence was sampled three times at different spatial intervals. Samples were initially collected with two cm spacing for bulk density, LOI, percent carbon and nitrogen, carbonate mineral stable isotope composition, and X-ray diffraction (XRD). Additional samples were collected at one cm resolution for LOI analyses, and continuous samples were collected from the Castor Lake core section above the Mazama tephra at an interval of two to three mm for isotope analysis of sedimentary carbonates. The Scanlon Lake cores were sampled at four to five cm spacing for bulk density, LOI, and XRD analysis.

3.5. Bulk density and loss-on-ignition

One-cubic centimeter samples were collected from the cores, weighed, then oven-dried at 60 °C and reweighed to determine wet and dry bulk density. The samples were combusted at 550 °C, weighed, combusted at 1000 °C, and weighed in order to determine the approximate weight percentages of organic matter, carbonates, and residual minerogenic components (Dean, 1974). The LOI weight percentage data were converted to sediment mass accumulation rate (MAR) values using continuous sedimentation rates (cm/yr) from the age models and bulk density measurements.

3.6. Organic carbon and nitrogen content

Measurements of the weight percentages of organic carbon and nitrogen in the Castor Lake sediment were conducted at the University of Alaska, Fairbanks School of Fisheries and Ocean Sciences. Sub-samples were acidified with 1 N HCl and rinsed to neutral, freeze dried and pulverized, for combustion to CO_2 and NO_2 by a Carlo-Erba CN elemental analyzer. The weight % C and % N results were converted to percent total organic carbon (TOC) and total nitrogen (TN) using the carbonate content data determined by LOI to correct for the relative mass fraction of carbonate that was removed from the sample via acidification. Molar ratios of TOC/TN content were calculated based on these data.

3.7. Carbonate mineral isotope values and XRD

Samples for carbonate mineral stable isotope and XRD analyses were disaggregated in 7% H_2O_2 for ~24 h, wet sieved through a 63 μm screen to remove the coarse fraction (and thereby isolate the fine grain size), and treated with 3% NaClO for 6 h to remove organic matter. The treated fine fraction was then rinsed three times using deionized water, frozen, lyophilized, and homogenized using a mortar and pestle.

The majority of the Castor Lake carbonate isotope analyses were conducted at the Regional Stable Isotope Laboratory for Earth and Environmental Science at the University of Pittsburgh using a dual-inlet GV Instruments, Ltd. (now Elementar UK Ltd.) stable isotope ratio mass spectrometer and MultiPrep inlet module. Measurements were calibrated to the NBS-18 and NBS-19 calcite standards, and values are reported in standard delta notation as the per mil deviation from Vienna Pee Dee Belemnite (VPDB). Precision (1σ) is ±0.1‰ for $\delta^{18}O$ and ±0.05‰ for $\delta^{13}C$ based on replicate measurements of NBS-18 and NBS-19 standards. Two carbonate isotope values were removed from the record due to low carbonate mineral content (<7.5% by mass as determined via LOI). Additional detail on carbonate stable isotope analyses is provided by Nelson et al. (2011).

Powder XRD analyses of six sediment samples from Castor Lake were performed at the University of Pittsburgh Materials Micro-Characterization Laboratory using a Phillips X-pert Powder Diffractometer over a 2θ range of 10°–80°. Nine samples from Scanlon Lake were analyzed at the University of Minnesota Duluth Research Instrumentation Lab using an identical instrument and method. X'Pert Graphics and Identify software was used to determine the mineral assemblages.

3.8. Significance of differences between mean proxy values from each time period

We conducted two-tailed t-tests to assess the statistical significance of the differences in mean $\delta^{18}O$ values from the time periods discussed in the text (i.e. 13,500 to 12,900 yr BP; 12,900 to 11,700; 11,700 to 7600; 7600 to 6200; and 6200 to present) (Table 4). The $\delta^{18}O$ series was interpolated at a ten year resolution, which is consistent with the average temporal resolution of the record. To account for redness in the data we adjusted the degrees of freedom by dividing the number of data points from each time period by the decorrelation time $(1 + \rho)/(1 - \rho)$, where ρ is the lag-1 autocorrelation.

4. Results and discussion

4.1. Sediment core lithology, age models, and time periods of interest

The Castor Lake composite sediment sequence spans a depth range of 448 cm and is divided into five lithologically distinct units (Fig. 6). The basal unit (unit C1, 420–448 cm) consists of laminated to finely banded, silicate minerogenic glaciolacustrine clay sediment. Laminated organic and calcareous silty clay (unit C2, 350–420 cm) overlies the basal unit, above which occurs fine to coarsely laminated calcareous silty clay (unit C3, 315.5–350 cm). Rhyolitic tephra from the Mazama eruption (285.5–315.5 cm) comprises unit C4. Mottled calcareous silty clay (unit C5, 256–285.5 cm) occurs above the Mazama tephra, while the remainder of the sediment sequence (aside from the MSH-W tephra centered on 53.2 cm) consists of fine to coarsely laminated calcareous silty clay (C3, 0–256 cm). The sedimentation rate at Castor Lake varied between 0.010 and 0.333 cm/yr, with a mean value of 0.030 cm/yr that is characteristic of the majority of the record. One ^{14}C control point located below the Mazama tephra produces an anomalously young age and was rejected in the Bchron age model. The highest sedimentation rates occur in the upper part of the sequence.

The Scanlon Lake composite sediment sequence spans a depth range of 673 cm and is divided into seven lithologically distinct units (Fig. 7). The base of the sediment sequence consists of laminated to homogenous, silicate minerogenic glaciolacustrine clay (unit S1; 630–673 cm), directly above which lies laminated organic and calcareous silt (unit S2, 489–630 cm). Rhyolitic tephra deposits from the Mazama climactic eruption (unit S3a, 480–489 cm) are proximately overlain by reworked tephra (unit S3b, 469–480 cm), mottled and homogeneous organic silty clay with terrestrial organic deposits containing root structures (unit S4, 450–469 cm), and homogeneous and mixed magnesium carbonate evaporite sediments with intermittent laminations (unit S5, 404–450 cm). The remainder of the sediment sequence consists of laminated to banded organic calcareous silty clay with magnesium carbonate laminations (unit S6, 323–404 cm) and fine to coarsely laminated

Table 3
XRD results.

Lake	Total depth (cm)	Median age (yr BP)	Major minerals present (abundance decreasing from left to right)
Castor	80	1120	aragonite
Castor	126.5	1890	aragonite
Castor	231	5180	aragonite
Castor	284	7500	aragonite, quartz
Castor	321	7900	aragonite, aluminosilicates
Castor	366	10140	aragonite, aluminosilicates
Scanlon	330.5	5840	aragonite
Scanlon	350.5	6210	Tremolite, Hibschite, Magnesium vanadium silicate
Scanlon	370	6580	hydromagnesite
Scanlon	391.5	6960	quartz, clinoenstatite
Scanlon	423	7200	aragonite, triplite
Scanlon	446	7340	huntite
Scanlon	468	7520	quartz, albite
Scanlon	512	8050	microcline, magnesium silicate
Scanlon	522	8230	quartz

Table 4
Significance values from t-tests.

Time Period[a]	6.2 – present	7.6–6.2	11.7–7.6	12.9–11.7
Significance values				
6.2 – present	1	–	–	–
7.6–6.2	<0.001	1	–	–
11.7–7.6	0.159	<0.001	1	–
12.9–11.7	<0.001	<0.001	<0.001	1
13.5–12.9	<0.001	0.004	<0.001	0.080
Difference between means (absolute value ‰)				
6.2 – present	0	–	–	–
7.6–6.2	1.64	0	–	–
11.7–7.6	0.12	1.76	0	–
12.9–11.7	4.88	6.52	4.76	0
13.5–12.9	4.48	6.12	4.37	0.40

[a] Thousands of years before present.

calcareous silt (unit S7, 0–323 cm), with the exception of the MSH-W tephra centered on a depth of 93.5 cm. Two of the 14 ^{14}C control points, both located above the MSH-W tephra, were rejected as outliers in the Bchron age model. Sedimentation rates at Scanlon Lake varied between 1.00 and 0.018 cm/yr with a mean value of 0.061 cm/yr. The highest sedimentation rates occur near the surface.

In the six Castor Lake samples analyzed using XRD, aragonite was the only carbonate mineral detected (Table 3), indicating that aragonite is likely the predominant carbonate mineral type present in the sediment. Furthermore, the magnesium concentration in Castor Lake water is high (Mg/Ca ratio > 9) (Steinman et al., 2013), and magnesium is known to strongly inhibit calcite formation (Sun et al., 2015). We therefore assert that the Castor Lake δ^{18}O record is not influenced by multiple carbonate mineral phases, while acknowledging that a more thorough XRD survey would be required to fully conclude that aragonite is the only carbonate mineral present. Non-aragonite related XRD peaks occur in the basal glaciolacustrine sediments, wherein terrigenous clastic content is greater, but these are attributable to the presence of quartz, albite, and other aluminosilicate minerals, as confirmed through smear slide analysis (Nelson, 2004). XRD profiles exhibit a gradual increase across the 2θ interval from ~10° to 20° in the non-laminated carbonate sequence that lies immediately above the Mazama tephra. This result suggests that amorphous opal concentrations, a characteristic feature of diatoms, are high in the post-

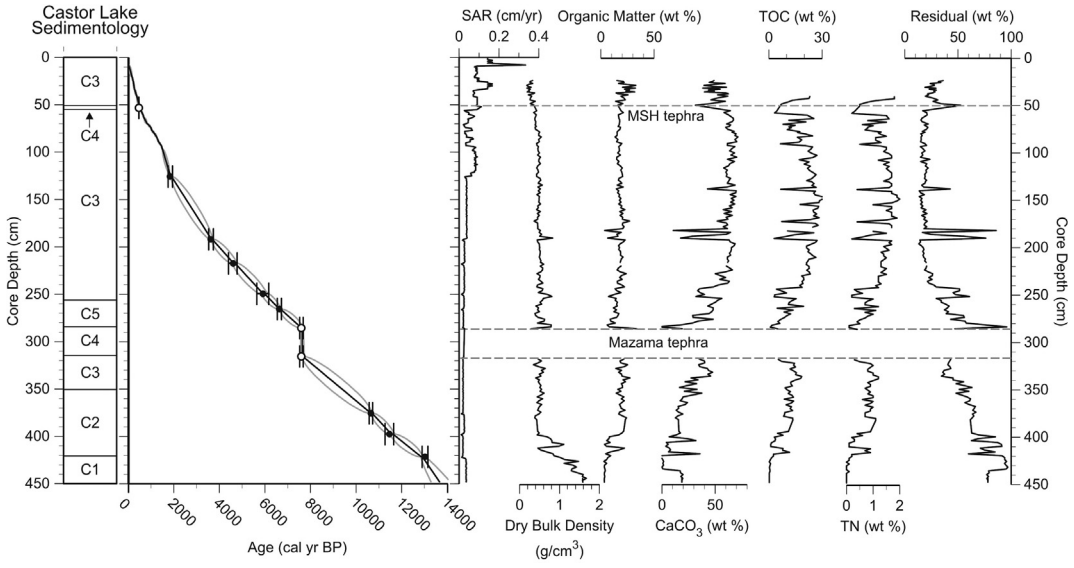

Fig. 6. Castor Lake (from left to right) stratigraphic column and age model depicting the median (black line), 90% uncertainty range (grey lines), control points (circles – open for tephra), and 2σ uncertainty range (brackets) for each control point; sediment accumulation rate (SAR); dry bulk density; and % weight results for organic matter (LOI), carbonate (LOI), total organic carbon, total nitrogen, and residual material (LOI). Lithologic units: C1 - laminated to finely banded, silicate minerogenic glaciolacustrine clay; C2 - laminated organic and calcareous silty clay; C3 - fine to coarsely laminated calcareous silty clay; C4 - rhyolitic tephra; C5 - mottled calcareous silty clay.

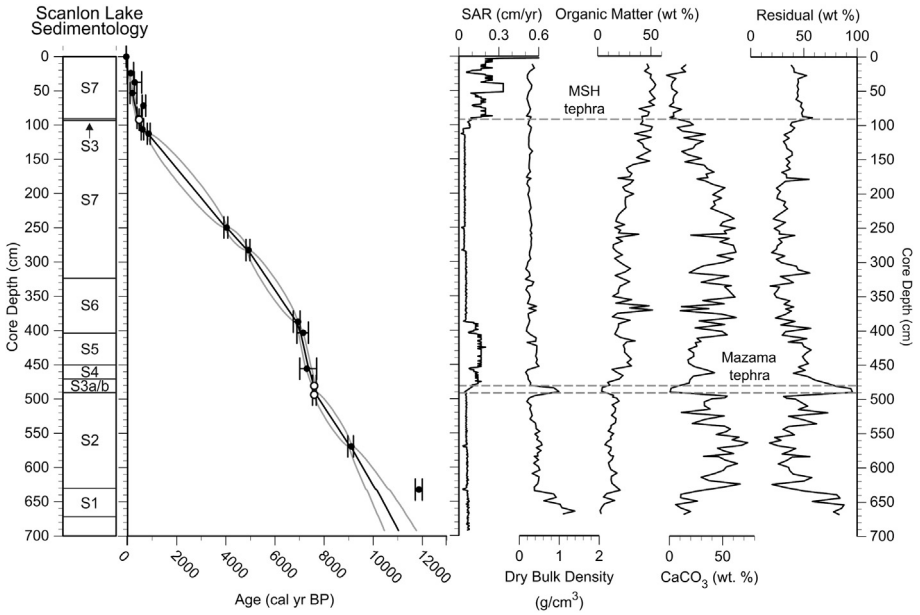

Fig. 7. Scanlon Lake (from left to right) stratigraphic column and age model depicting the median (black line), 90% uncertainty range (grey lines), control points (circles – open for tephra), and 2σ uncertainty range (brackets) for each control point; sediment accumulation rate (SAR); dry bulk density; and LOI results as % weight. Lithologic units: S1 - laminated to homogenous, silicate minerogenic glaciolacustrine clay; S2 - laminated organic and calcareous silt; S3a - rhyolitic tephra; S3b - reworked tephra; S4 - mottled and homogeneous organic silty clay with terrestrial organic deposits containing root structures; S5 - homogeneous and mixed, magnesium carbonate evaporite sediments with intermittent laminations; S6 - laminated to banded organic calcareous silty clay with magnesium carbonate laminations; S7 - fine to coarsely laminated calcareous silt.

Mazama tephra deposits in Castor Lake. XRD analyses of Scanlon sediment indicate various carbonate minerals including aragonite, hydromagnesite ($Mg_5(CO_3)_4(OH)_2{\cdot}4H_2O$; hydrated magnesium carbonate), and huntite ($Mg_3Ca(CO_3)_4$; magnesium carbonate), the latter two of which occur primarily in the mottled, calcareous silty clay unit directly above the Mazama tephra.

Results from the significance tests (Table 4) indicate that the mean $\delta^{18}O$ values from each time period are significantly different from one another (at the $p < 0.1$ level), with the exception of the difference between the 6200 to present and 11,700 to 7600 yr BP time periods. These two intervals, however, exhibit substantially different $\delta^{18}O$ trends, with the former varying between a range of −7.2 and −3.2‰ (~4‰) and the latter varying between −9.2 and −2.8‰ (>6‰) as well as containing the most positive values of the early Holocene.

4.2. Paleoproxy interpretation

The temporal evolution of the isotopic composition of lake water is controlled by a variety of processes including ocean/atmosphere circulation dynamics and lake/catchment hydrologic characteristics (Craig and Gordon, 1965; Gat, 1996). The isotope values of water bodies influenced by evaporation define a local evaporation line (LEL), which typically has a lower slope than the local meteoric water line (LMWL) (Gat, 1996) (Fig. 3). The LMWL is defined by the isotope values and seasonal isotopic variability of local meteoric water. Changes in temperature, relative humidity, cloud cover, and both synoptic and local scale atmospheric processes affect the isotopic composition of precipitation and regional evaporation rates, and thereby influence the isotope content of water bodies (Araguás-Araguás et al., 2000; Craig and Gordon, 1965; Gat, 1996). Changes in the seasonal distribution and amount of precipitation are an additional strong control on lake water isotope values (Henderson and Shuman, 2009; Steinman et al., 2016).

There are three ways through which lakes can lose water: evaporation, overflow, and outseepage through the lake bed. Of these, only evaporation is a fractionating process that directly affects the lake water isotope content (Steinman and Abbott, 2013). Closed-basin lakes lose a substantial amount of water through evaporation and hence are isotopically enriched relative to meteoric water. Open-basin lakes that are minimally affected by evaporation have water isotope values consistent with meteoric water. In closed-basin lakes, the water isotopic composition will vary in response to the proportion of water lost through evaporation, with greater ^{18}O and ^{2}H concentrations associated with lesser precipitation and/or greater evaporation amounts, and vice versa (Benson and Paillet, 2002; Jones and Imbers, 2010; Shapley et al., 2008; Steinman et al., 2013; Steinman and Abbott, 2013). In contrast, the water isotope composition of open-basin lakes exhibits little to no ^{18}O or ^{2}H enrichment, plotting along the LMWL and mirroring that of inflowing meteoric water (precipitation and catchment groundwater inflows) (Fig. 3).

Lacustrine carbonate minerals that form in isotopic equilibrium with lake water provide an archive of lake water oxygen isotope values at the time of mineral formation. Carbonate mineral isotope content is a particularly insightful proxy because the biological and chemical processes that control the formation and isotopic composition of authigenic carbonates are well understood (Kelts and Talbot, 1990; Talbot and Kelts, 1990). Furthermore, alkaline lakes that precipitate carbonate minerals are relatively common, spanning a wide geographic distribution and range of elevations. When combined with chronological assessment, the analysis of $\delta^{18}O$ values in authigenic carbonate sediment can provide records of past changes in paleoclimatic and paleolimnological variables including lake level, catchment water balance, the source of atmospheric moisture, and (in some settings) temperature (Leng and Marshall, 2004), depending on the hydrologic characteristics of the study lake.

Observational data and modeling results indicate that Castor

Lake and Scanlon Lake are hydrologically closed, with water isotope compositions that predominantly reflect changes in lake level resulting from variations in precipitation and evaporation (Steinman et al., 2010b). Isotope values in both lakes are also influenced by changes in the isotopic composition of meteoric water inputs, although this effect is secondary, due to the low magnitude of interannual isotopic variability of meteoric water (Steinman and Abbott, 2013). The Castor Lake sediment oxygen isotope record can therefore be interpreted to principally reflect past changes in water oxygen isotope values resulting from variations in catchment hydrologic inputs (i.e. runoff and baseflow) and consequent changes in lake level.

The carbon isotopic composition of lacustrine carbonates is primarily controlled by the carbon isotope content of lake water DIC, which is affected by several processes including atmospheric exchange, the $\delta^{13}C$ values of DIC in catchment and groundwater inflow, recycling of organic matter within the sediments and water column, and the total concentration of DIC in both lake water and inflowing catchment/ground water (Li and Ku, 1997; Talbot, 1990; Talbot and Kelts, 1990). Closed-basin lake carbonate mineral $\delta^{13}C$ and $\delta^{18}O$ values often exhibit covariance as a result of the influence of changes in hydrologic balance and residence time on the isotopic composition of water and DIC (Horton et al., 2016; Li and Ku, 1997). The carbon isotopic composition of groundwater DIC is typically depleted relative to that of lake water as result of the oxidation of isotopically light terrestrial organic matter and dissolution of the resulting CO_2. We interpret the Castor Lake carbonate mineral $\delta^{13}C$ record principally as an indicator of precipitation-evaporation balance and the resulting isotopic effects on lake DIC and secondarily as an indicator of the extent of sediment organic matter oxidation (particularly during prolonged lowstands during which bottom water is oxygenated). The $\delta^{18}O$ and $\delta^{13}C$ data from Castor Lake generally exhibit a positive covariance on both shorter and longer time scales, indicative of long-term closed-basin hydrology (Li and Ku, 1997; Talbot, 1990), and thereby support our assertion of hydrologic balance control on $\delta^{13}C$ values. In sediments from the middle Holocene, however, a strongly negative covariance occurs, although this can be explained to have resulted from changes in lake level (as discussed below).

The carbon and nitrogen content of lake sediment is controlled by organic matter deposition, degradation, and productivity rates and hence is influenced by a variety of terrestrial and aquatic processes. The TOC/TN ratio of organic sediment is primarily controlled by the relative proportion of terrestrial (TOC/TN > 20) versus aquatic (TOC/TN < 10) source inputs (Meyers and Teranes, 2001) and secondarily by changes in the TOC/TN ratio of both terrestrial and aquatic source matter. We interpret the organic sediment carbon and nitrogen content results (along with the LOI organic weight percent and flux data) as an indicator of total organic matter deposition and preservation and the TOC/TN ratio as a reflection of the relative contributions of terrestrial versus aquatic organic matter to the sediment.

4.3. Paleoenvironmental reconstruction

4.3.1. Deglaciation and the Younger Dryas (~13,500 to 11,700 yr BP)

The area surrounding Castor Lake was last glaciated during the Fraser advance of the late Pleistocene when the thickness of the Okanogan lobe of the Cordilleran ice sheet reached ~2000 m in this location (Waitt and Thorson, 1983). The distribution of tephra layers associated with the Glacier Peak G eruption (13,430 yr BP) (Foit et al., 1993; Kuehn et al., 2009) indicates that the southern Okanogan River basin was likely ice free by ~13,000 yr BP (Clague and James, 2002; Waitt and Thorson, 1983). The Castor Lake sediments from this time mostly consist of laminated glaciolacustrine clays (Fig. 6), as reflected by the high LOI residual MAR values and low organic matter amounts from 13,560 to 12,990 yr BP (Fig. 8), indicating that Castor Lake formed in a periglacial landscape. LOI residual values (i.e. clastic mineral material) begin a sharp decline at 12,990 yr BP, likely as a result of the progressive establishment of catchment vegetation, which stabilized the glacial outwash sediments and reduced fluvial erosion. The TOC/TN ratio increases after deglaciation to a value of 16.8 at 12,990 yr BP (Bchron 90% range: 12,860–13,210 yr BP; this format is applied hereafter to all age uncertainty ranges), perhaps reflecting the initial expansion of terrestrial vegetation after deglaciation.

The Younger Dryas cold reversal spanned ~12,900 to 11,700 yr BP, as indicated by temperature records from ice cores and other paleorecords (Andersen et al., 2004; Lohne et al., 2014, 2013; Muschitiello and Wohlfarth, 2015; Rasmussen et al., 2006), and is not distinctly expressed in the Castor Lake sediment by all proxies. Instead, a low organic matter flux from 12,860 (12,780–12,960) to 11,440 (11,240–11,620) yr BP, a high residual flux from 12,210 (11,850–12,540) to 11,690 (11,490–11,940) yr BP, and highly variable TOC/TN values occur (Figs. 6 and 8). A sediment facies transition from glaciolacustrine clay to laminated organic and calcareous silty clay occurs at a depth of 420 cm, corresponding to 12,750 yr BP. We suggest this lithostratigraphic transition reflects a period of landscape instability associated with the progressive erosion of glacial till from the catchment into the lake. The low organic matter content and the increase in LOI residual MAR values, which peak 650 years (at 12,100 yr BP) after the sediment facies transition, is consistent with a reduction in terrestrial vegetation, the destabilization of catchment sediment, and consequent increases in the delivery of minerogenic sediment to the lake in response to the reestablishment of a glacial-like (presumably cold, windy, and dry) climate. The initial increase in the TOC/TN ratio (from 13.9 at 12,860 yr BP to 18.8 at 12,620 yr BP), and subsequent decline (to a value of 10.7 at 12,310 yr BP) indicate that primary productivity may have declined at the onset of the Younger Dryas, and then subsequently increased perhaps due to changes in nutrient delivery. Anomalous peaks in TOC and TN MAR occur at 12,510 (12,180–12,760) yr BP, suggesting that vegetation die off associated with colder temperatures may have temporarily increased the terrigenous flux of organic matter and nutrients to the lake. The utility of the Castor Lake $\delta^{18}O$ and $\delta^{13}C$ records from the Younger Dryas (Fig. 9) is limited by a relatively low carbonate mineral content (<1% in some intervals) (Fig. 6) and consequent lack of reproducibility in the isotope data for this time period. Nevertheless, $\delta^{18}O$ and $\delta^{13}C$ values are the lowest of the record, suggesting that lake levels were high, perhaps in response to greater runoff due to poorly developed soils and vegetation, and consequently lower rates of both water retention in the catchment and losses through evapotranspiration.

4.3.2. Early Holocene climate/environmental variability (11,700 to 7600 yr BP)

Following the Younger Dryas termination, ecological conditions at Castor Lake appear to have shifted, as indicated by an increase in total organic matter, TOC, and TN MAR from 11,360 to 10,820 yr BP and the continuation of a decreasing trend in residual minerogenic content that begins at 12,100 yr BP (Fig. 8). These changes suggest increased organic matter delivery to the lake, perhaps in response to the expansion of catchment vegetation and/or greater productivity. The lack of an abrupt change in the TOC/TN ratio may be a result of the competing effects of greater lake productivity, which would reduce the lake sediment TOC/TN ratio, and greater terrestrial vegetation inputs to the lake, which would produce a higher TOC/TN ratio.

Organic matter, TOC, and TN MAR are somewhat stable between

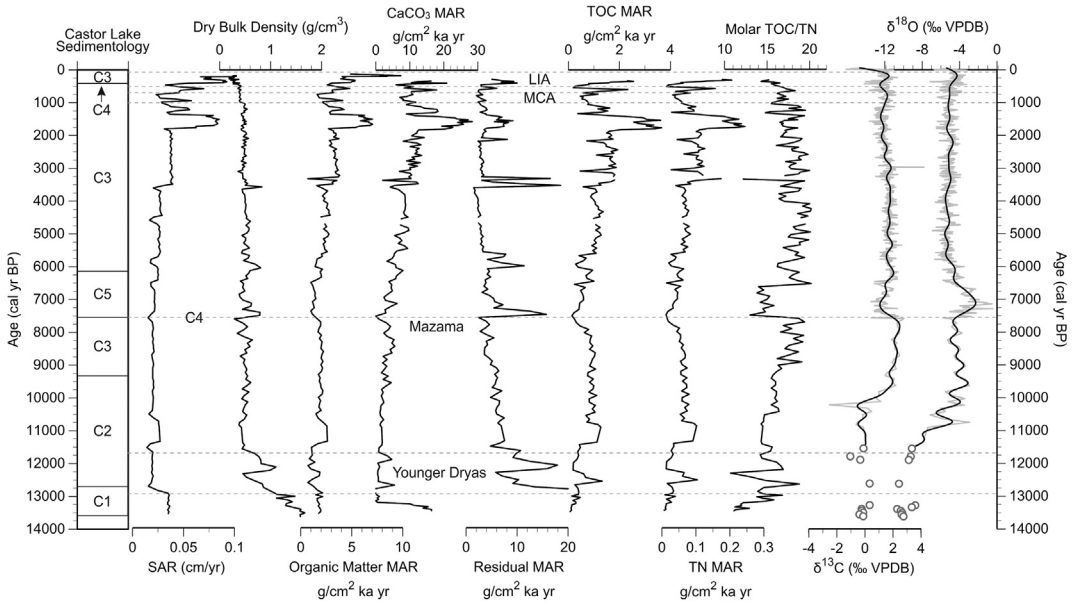

Fig. 8. Castor Lake sediment accumulation rate (SAR), dry bulk density, organic matter MAR, carbonate mineral MAR, residual material MAR, TOC MAR, TN MAR, and Molar TOC/TN data. Horizontal grey lines mark tephra and the time periods referenced in the text. Lithologic descriptions are the same as shown in Fig. 6.

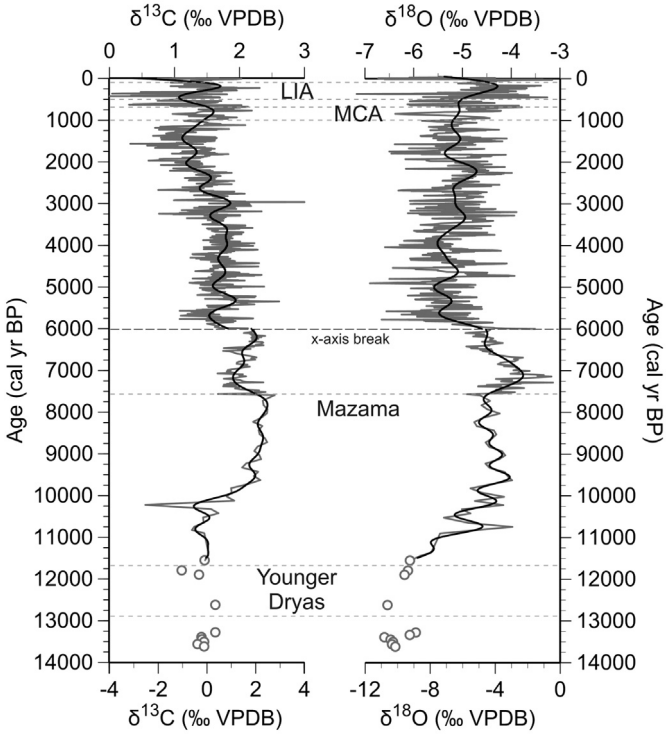

Fig. 9. Castor Lake carbonate mineral $\delta^{18}O$ and $\delta^{13}C$ data (grey lines) and 500 year lowpass filtered time series (black lines) (Mann, 2008). Horizontal grey lines mark tephra and the time periods referenced in the text. There are two x-axes, with the break at 6000 yr BP.

10,820 and 7600 yr BP (Fig. 8), likely due to the establishment and gradual evolution of the lake/catchment ecosystem, an inference that is supported by constancy in the pollen records from Mud Lake (8.2 km northwest of Castor Lake; elevation 650 m) and Bonaparte Meadows (46 km northeast of Castor Lake; elevation 1050 m) (Fig. 1) (Mack et al., 1979). The increase in TOC/TN over this interval suggests a greater terrestrial contribution to the sediment organic matter, likely derived from newly developed catchment soils, an inference supported by the decline in residual minerogenic inputs to the lake. Coincidentally, sediment organic matter contributions from aquatic sources and preservation must also have declined in order to maintain the steady organic matter and TOC MAR values.

$\delta^{18}O$ increases by ~6‰ (with substantial variability) between 11,700 and 9630 yr BP, at which point values begin to decline until after the Mazama tephra deposition at ~7600 yr BP (Fig. 9). The early Holocene maximum in oxygen isotope values at 9630 (9110–10,100) yr BP, which notably is preceded by a positive anomaly at 10,750 yr BP, indicates that dry conditions and lower lake levels likely prevailed at this time in response to lower precipitation amounts and/or greater evaporation rates. The timing of the peak in $\delta^{18}O$ is approximately consistent with a lithological shift from more organic to more calcareous laminae at a depth (350 cm) corresponding to 9380 yr BP. The abundance of laminae in the early Holocene sediment indicates that the hypolimnion was primarily anoxic (Fig. 6), perhaps in part as a result of wind protection provided by the steep sided catchment, which limits wind driven mixing and deepening of the epilimnion.

4.3.3. Middle Holocene lowstand and the Mt. Mazama eruption (7600 to 6200 yr BP)

The Castor Lake sediment record suggests that immediately after the deposition of the Mt. Mazama tephra at ~7600 yr BP (Hallett et al., 1997; Zdanowicz et al., 1999) substantial changes occurred in lake/catchment ecology and hydrologic balance. The Plinian climactic eruption was a cataclysmic event that created Crater Lake in southwest Oregon (~660 km south/southwest of Castor Lake) (Fig. 1) and deposited a thick ash layer (five to ten cm compacted) in eastern Washington (Hoblitt et al., 1987). The Castor Lake sediment facies stratigraphically above and below the tephra are markedly different, with the lower unit characterized by laminated calcareous silty clay and the upper sediments by mottled calcareous silty clay (Fig. 10). We suggest this abrupt transition indicates that lake levels declined after the eruption to an extent sufficient to oxygenate the bottom water. Lithological changes in sediment facies from Scanlon Lake provide further evidence that lake levels were substantially lower after the eruption. For example, five cm

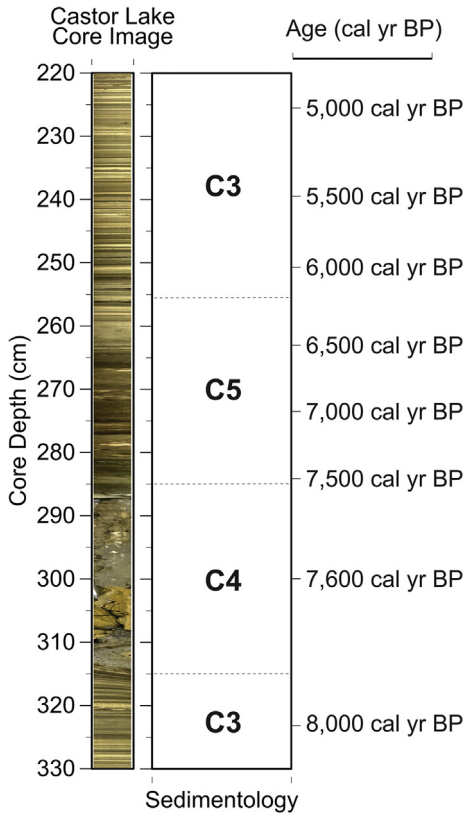

Fig. 10. Middle Holocene lithostratigraphic facies column for Castor Lake. Lithologic units: C3 - fine to coarsely laminated calcareous silty clay; C4 - rhyolitic tephra; C5 - mottled calcareous silty clay.

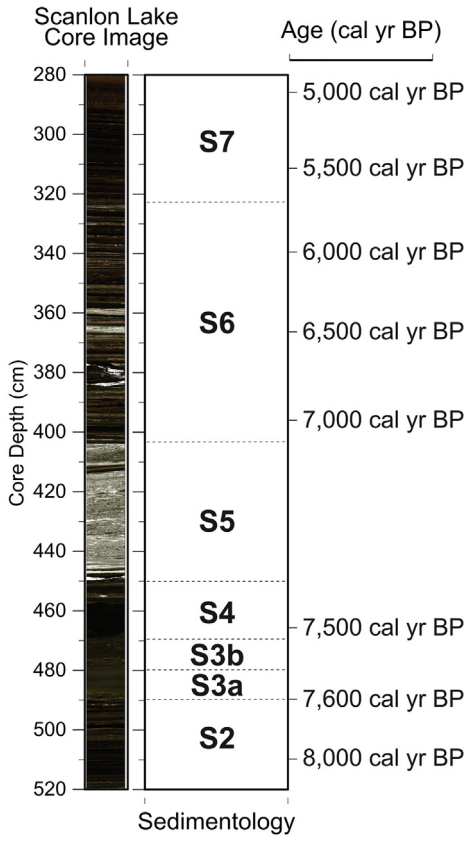

Fig. 11. Middle Holocene lithostratigraphic facies column for Scanlon Lake. S2 - laminated organic and calcareous silt; S3a - rhyolitic tephra; S3b - reworked tephra; S4 - mottled and homogeneous organic silty clay with terrestrial organic deposits containing root structures; S5 - homogeneous and mixed, magnesium carbonate evaporite sediments with intermittent laminations; S6 - laminated to banded organic calcareous silty clay with magnesium carbonate laminations; S7 - fine to coarsely laminated calcareous silt.

above the Mazama tephra in Scanlon Lake the sediment transitions to a ~12 cm thick layer of highly cohesive, low density organic matter with an upper surface age of 7410 (7290–7530) yr BP (Fig. 11). This layer, which contains abundant root structures, is unique in the context of the Scanlon Lake sediment record and must have formed when lake levels were very low and the sill separating the two basins (Fig. 1) was subaerially exposed. Above the lowstand layer the Scanlon Lake sediment abruptly changes to homogenous and mixed silty clays containing magnesium carbonates (hydromagnesite and huntite) (Table 3) that likely formed as a result of high concentrations of magnesium and carbonate/bicarbonate during periods of high salinity. The Mg/Ca ratio of Scanlon Lake water has been observed to exceed 140 (Steinman et al., 2013), a value greater than the level required for the formation of high magnesium carbonates (Müller et al., 1972). These complementary lines of evidence from Castor Lake and Scanlon Lake conclusively demonstrate that a substantial lowering of lake levels occurred within several decades to centuries subsequent to the Mazama eruption.

Abrupt changes in $\delta^{18}O$ and $\delta^{13}C$, residual and organic matter content, and TOC/TN at ~7,600 yr BP are coincident with the shifts in Castor Lake and Scanlon Lake sedimentology and support the assertion that lake levels declined and that lake/catchment environmental conditions were considerably altered in response to, or occurring synchronously with, the Mazama tephra deposition. $\delta^{18}O$ increases by ~4.5‰ over ~300 years following the eruption, confirming the shift to lower lake levels (Fig. 9). The maximum oxygen isotope value (of −0.4‰) occurs at 7290 (7020–7500) yr BP and is followed by a short interval of lower values before increasing to the highest sustained values of the record (multiple consecutive data points greater than −1.7‰) from 7160 (6890–7410) to 7090 (6830–7350) yr BP, indicating the lowest lake levels of the Holocene between 7290 and 7090 yr BP. Castor Lake sediment residual minerogenic content and bulk density increase immediately after the eruption and remain high for ~200 years as a result of the erosion of ash from the catchment and deposition into the lake (Fig. 8). Smear slides confirm the increase and subsequent decline in the concentration of volcanic glass after the tephra deposition, and additionally reveal a large increase in the concentration of diatoms and other siliceous organisms (Nelson, 2004) likely resulting from an increase in diatom productivity in response to a greater silica influx (Telford et al., 2004). The post-eruption decrease in organic matter is partially attributable to enhanced decomposition resulting from greater oxygen concentrations at the sediment water interface (Meyers and Teranes, 2001). The decrease in TOC/TN (from 18.7 to 13.0) between 7600 and 7480 yr BP indicates a major shift in sediment organic matter composition toward relatively greater amounts of aquatic biomass. This likely resulted from greater productivity and possibly from a decline in terrestrially derived organic matter (Meyers and Teranes, 2001). The pronounced decline in carbonate $\delta^{13}C$ values immediately following the eruption might be viewed as contradictory to the interpretation of enhanced productivity, given that increased photosynthetic activity in the lake water should enrich the $\delta^{13}C$ value of the residual DIC pool (Li and Ku, 1997). However, the reduction of water column stratification during the lowstand interval would have countered

this effect, as stratified conditions are a required component for most productivity driven mechanisms that describe carbon isotope variations in lake water (Diefendorf et al., 2008; Hammarlund et al., 1997; Hodell et al., 1998; Meyers and Teranes, 2001). We suggest that the non-stratified water column may have allowed for increased remineralization of organic matter under aerobic conditions and consequent re-introduction of isotopically light carbon from sediments to the DIC pool during the lowstand. This suite of sediment geochemistry data provides a detailed perspective on the timing of lake-level and environmental change in the Castor lake/catchment system that is supported by the more general lake-level change inferences derived from analyses of sedimentary facies.

The transition to higher lake levels following the post-Mazama lowstand produced major changes in sediment geochemistry that reflect considerable variability in lake/catchment environmental processes. Castor Lake $\delta^{18}O$ values follow a generally declining trend but remain high overall from 7090 to 6420 yr BP, indicating that lake levels were low but gradually increasing (Fig. 9). The TOC/TN ratio is low through this interval until abruptly increasing at 6630 yr BP, broadly consistent with the timing of the $\delta^{13}C$ increase at 6530 yr BP (Fig. 8). This implies that a threshold response in carbon cycling occurred in response to the increase in lake levels that followed the post-Mazama lowstand. One possibility is that higher lake levels promoted more consistent thermal stratification. This would have reestablished bottom water anoxia, and in essentially the reverse of the mechanism proposed above, resulted in reduced respiration and remineralization of organic matter at the sediment water interface (Meyers and Teranes, 2001), effectively decreasing nutrient delivery to the surface water. The reduced benthic nutrient recycling would have thereby limited productivity and led to an increase in the TOC/TN ratio (due to a relative increase in terrestrial versus aquatic matter fluxes) and an increase in $\delta^{13}C$ values (resulting from the decline in $\delta^{13}C$ depleted organic matter oxidation in lake bottom water). Collectively these results indicate that multi-decadal (or longer) scale shifts in lake carbon cycling and organic matter production/preservation in sediment can occur when long-term changes in lake level trigger threshold responses, and that such changes occurred at Castor Lake in the centuries following the Mazama eruption.

The end of the middle Holocene lowstand occurred at 6190 yr BP (5960–6410) yr BP (depth of 256 cm), as indicated by the transition in the Castor Lake record from banded, mottled stratigraphy to laminated sediment (Fig. 10) and the $\delta^{18}O$ decline to values consistent with those from prior to the Mazama eruption (Fig. 9). TOC, TN, and organic matter MAR values and the TOC/TN ratio achieve localized maxima centered on ~6200 yr BP, indicating either a greater influx of terrestrial organic matter (perhaps due to increased precipitation and runoff), greater organic matter preservation, or some combination of the two in association with higher lake levels and more stable stratification/oxygen-poor bottom waters than had occurred in the prior several centuries (Meyers and Teranes, 2001) (Fig. 8). The Scanlon Lake sediment facies suggest a similar pattern, with a transition at 6710 yr BP (depth of 377 cm) from mixed magnesium carbonates to laminated aragonite/calcite layers that characterize the remainder of the Holocene sequence above (Fig. 11). The disparity between the timing of the lithology transitions at Castor Lake and Scanlon Lake is likely due in part to the differences in water depth at the core location (i.e. the Scanlon Core is from a shallow location, 2.5 m, whereas the Castor Lake core is from a deep location, 11.5 m), lake stratification and basin morphology at the two sites and the consequent effects on the establishment and persistence of bottom water anoxia. For example, there are several magnesium carbonate mineral layers in the Scanlon Lake record above the transition from mixed to laminated sediment, suggesting that lake water magnesium and carbonate ion concentrations remained high as a result of low lake levels for several centuries after the timing of the facies change.

There are several possible explanations for the post-Mazama lowstand that involve changes in climate and/or effects of ash deposition on catchment hydrology. One possibility is that the lower lake levels were caused by a relatively rapid change in climate, perhaps in response to orographic feedbacks related to the position of central Washington in the continental interior between the Cascade and Rocky Mountain ranges, while simultaneously elsewhere in the Pacific Northwest the climate response was more gradual. That such an abrupt shift has not been identified in other records makes this the least plausible explanation. A second possibility is that lake levels gradually declined, but the sedimentological and geochemical response was non-linear and abrupt. This is an unlikely explanation as well, in light of lake hydrologic and isotope mass balance modeling experiments that do not demonstrate a threshold type oxygen isotope response to declining lake levels (Jones and Imbers, 2010; Shapley et al., 2008; Steinman et al., 2016; Steinman and Abbott, 2013). A third possibility is that the Mazama ash deposition was directly and exclusively responsible for the lowstand through effects on lake/catchment hydrology. More specifically, the tephra and its weathering products may have increased catchment water retention capacity and soil evaporation, thereby reducing runoff and lowering lake levels (as described below). The fourth, and most plausible, explanation is that lake levels were already low in the decades/centuries prior to the Mazama eruption in response a dry climate related to large scale changes in atmospheric circulation (Bartlein et al., 2014; Hebda, 1995; Whitlock, 1992), and that deposition of the tephra enhanced the lowstand through effects on catchment hydrology.

The geochemical characteristics of soils derived from volcanic ash support the idea of potential hydrologic impacts resulting from deposition of the Mazama tephra. Andisols, or soils that form in volcanic ash have a high porosity (and low bulk density), derived in part from the abundance of porous, permeable, vesicular volcanic glass. This results in a high water retention capacity (Neall, 2006; Ping, 2000) that is enhanced by the presence of a colloidal fraction derived from the weathering of ash. As such, ash cap horizons can have a substantially (in some cases two times) greater water holding capacity as lower horizons (Geist and Strickler, 1978; McDaniel et al., 2005; McDaniel and Wilson, 2007; Meurisse et al., 1991). In distal regions (such as north-central Washington relative to Mt. Mazama), ash fall is typically silt sized, which promotes the formation of silt-loam textures that further increase soil water retention (McDaniel and Wilson, 2007). The deposition of a finely textured ash on more coarsely textured soils therefore has the potential to increase catchment water retention, reduce runoff and thereby cause a decline in lake levels.

The modern soil taxonomy of the Castor and Scanlon lake catchments supports the hypothesis that substantial changes in lake hydrological regimes occurred in response to the Mazama ash fall. The predominant soil types in the Castor and Scanlon lake catchments are Lithic Xerochrepts of the Vallan Complex and Donovan Complex loams, along with substantial coverage by rock outcrops (NCSS, 2006). The Vallan Complex consists of shallow soils formed in colluvium and residuum from the weathering of rhyodacite and andesite (consistent with the Mazama ash composition) with a minor component of glacial till (USDA and NRCS, 2017). The Donovan Complex consists of well drained soils formed in mixed volcanic ash above glacial till (USDA and NRCS, 2017). Neither the Vallan or Donovan Complex soils are Andisols, due to their lack of a thick, undisturbed ash mantle, but rather are andic/vitrandic intergrades principally derived from volcanic ash and its weathering products (McDaniel et al., 2005). These soils therefore evolved from the precursor soils that formed in the centuries following the

Mazama eruption and that substantially altered the water retention capacity of the Castor Lake and Scanlon Lake catchments, at least for several centuries following the ash deposition. Further support for this hypothesis is provided by the lack of modern Andisol development in drier, non-forested and steep sided catchments subject to more active slope processes such as erosion and colluviation, conditions that favor ash removal from the catchment and the lack of an ash mantle (Briggs et al., 2006). The Castor and Scanlon Lake catchments have these characteristics and therefore were likely unable to support the full development and preservation of ash capped soils following the Mazama ash deposition.

The timing of shifts in the Castor Lake oxygen isotope record, as well as changes in sedimentological characteristics, provide insight into the rates of ash weathering, erosion, and incorporation into soils. Castor Lake $\delta^{18}O$ values decline by 0.8‰ immediately after the eruption and then increase by a maximum of 5.2‰ over the course of ~400 years (Fig. 9). The initial decline in $\delta^{18}O$ values may have resulted from a short-lived increase in lake level due to a temporary increase in runoff caused by ash deposition and vegetation die-off. Observational studies have demonstrated that catchment runoff typically increases immediately following ash deposition due to the ease with which thin ash layers can become saturated and the lack of hydraulic flow between the ash layer and underlying soil (Leavesley et al., 1989; Miller and Gardner, 1962; Ogawa et al., 2007; Pierson and Major, 2014), an effect that dissipates as erosion begins to remove the ash, vegetation becomes reestablished, and the ash is mixed into the layers below (Major and Yamakoshi, 2005; Pierson and Major, 2014). The stabilization of catchment vegetation likely occurred quickly, on the order of years to several decades, given that the ash thickness (compacted) was approximately five to ten cm (given the distance of ~660 km from Castor/Scanlon lake to Mt. Mazama) (Hoblitt et al., 1987) and that most trees and larger shrubs would have survived the initial depositional event (Antos and Zobel, 1986a, 1986b; Pfitsch and Bliss, 1988; Zobel and Antos, 1997). The progressive reestablishment of low lying vegetation would have slowed erosion rates and thereby promoted ash retention and weathering to clays on the landscape, which would have further increased catchment water retention capacity and reduced runoff. The Castor Lake sediment residual MAR and bulk density trends (Figs. 6 and 8) support this inference, exhibiting a pronounced increase directly after the eruption and maximum values prior to the peak in $\delta^{18}O$ (with a separation of ~340 years). During this time, the ash and its weathering products were probably slowly incorporated into the surface horizon through pedoturbation while simultaneously being eroded from the catchment. The subsequent increase in lake levels beginning at ~7100 yr BP (as indicated by the onset of the decline in $\delta^{18}O$) likely began once the formation of clays via weathering slowed (due to the reduction in parent ash material) to the extent that the effect on catchment water retention capacity of additional clay production was exceeded by the hydrological effects of ash (and clay) removal through erosion. At this point catchment water retention would have started to decrease with a concomitant lake level increase reflected by declining $\delta^{18}O$ values.

4.3.4. Middle through late Holocene climate/environmental variability (6200 yr BP to present)

Variations in the Castor Lake environmental proxies from 6200 yr BP to present indicate that substantial changes in the lake/catchment ecosystem occurred, although less so than during the post-Mazama eruption interval. The terrestrial organic matter flux likely increased from ~6000 to 4000 yr BP, as evinced by the increase in LOI organic, TOC, and TN MAR and TOC/TN ratios (Fig. 8). Low TOC/TN ratio values centered on ~4000 yr BP signal a decline in the proportion of terrestrial versus aquatic organic matter delivery, although TOC, TN, and LOI organic MAR values do not abruptly shift at this time, but rather continue to gradually increase, with a marked enhancement of shorter timescale variability after ~3700 yr BP. One possible explanation is that terrestrial organic contributions to the lake declined after 4000 yr BP, perhaps in response to the gradual drying of the cold season from the middle Holocene to present (Steinman et al., 2016). The Castor Lake $\delta^{18}O$ data support this assertion, varying about a mean value that is stable between ~5800 and 5000 year BP and that increases thereafter, with the highest values of the late Holocene occurring in the most recent millennium (Fig. 9).

The subtle, general decline in the TOC/TN ratio that begins at ~2500 yr BP suggests that primary productivity may have increased over this interval, perhaps in combination with a reduction in terrestrial organic matter influx. The large magnitude increases in MARs centered on 1600 yr BP and their subsequent declines until ~1000 yr BP are largely the result of a greater sediment accumulation rate during this time and therefore are likely an artifact of age model uncertainty, an assertion supported by the lack of similar magnitude responses in weight % values of the proxies. $\delta^{13}C$ values decline between 3000 and 1600 yr BP perhaps as a result of the gradual lowering of lake levels and the oxidation of sediment organic matter in accordance with the process (outlined above) invoked to explain the $\delta^{13}C$ trend during the post-Mazama lowstand (Fig. 9). $\delta^{13}C$ values increase from ~1500–650 yr BP then decline for several hundred years before returning to more positive values, a pattern that may reflect changes in productivity. However, the small magnitude of late Holocene changes in $\delta^{13}C$ are difficult to interpret given the myriad controls on lake water DIC isotope values (Horton et al., 2016; Li and Ku, 1997; Meyers and Teranes, 2001) and the lack of consistency with the other proxies in the Castor Lake record. The last 2000 years of the Castor Lake $\delta^{18}O$ record suggests wetter conditions during the Medieval Climate Anomaly (~1050–650 yr BP) and a relatively drier Little Ice Age (~500–100 yr BP), assertions that are explored in detail by Steinman et al. (2014, 2012) (Fig. 9).

4.4. Paleoenvironmental comparison

4.4.1. Deglaciation and the Younger Dryas (~13,500 to 11,700 yr BP)

The regional timing of the Younger Dryas cold reversal is well defined by the Oregon Caves National Monument (OCNM) speleothem record, wherein $\delta^{18}O$ values were lower (isotopically more negative) due to inferred colder atmospheric temperatures between $12{,}840 \pm 200$ and $11{,}700 \pm 260$ yr BP (Fig. 12) (Ersek et al., 2012; Vacco et al., 2005). Presumably, this temperature shift was accompanied by large changes in atmospheric and ocean circulation that had a profound effect on the hydroclimatology of the Pacific Northwest. For example, alpine glaciers on Mount Rainier retreated during the Younger Dryas, probably due to a decrease in precipitation while conditions remained cold (Heine, 1998). The multi-proxy lake sediment record from Castor Lake also indicates that changes in lake/catchment hydrologic and ecosystem characteristics occurred during the Younger Dryas (Fig. 8) in response to a return to cold and dry conditions similar to those of the deglacial period. The organic (TOC and TN MAR, TOC/TN) and sedimentological (organic matter and residual MAR) data suggest a reduction in terrestrial vegetation, increases in catchment instability and clastic sediment delivery as well as (potentially) shifts in aquatic productivity. $\delta^{18}O$ values are the most negative of the record (minimum of −10.8‰) during the Younger Dryas and preceding deglacial time period (in comparison with a value of −3.0‰ at 9630 yr BP). This cannot be entirely explained by changes in the isotopic composition of precipitation, which declined by less than ~1‰ as indicated by the OCNM speleothem data. A more likely

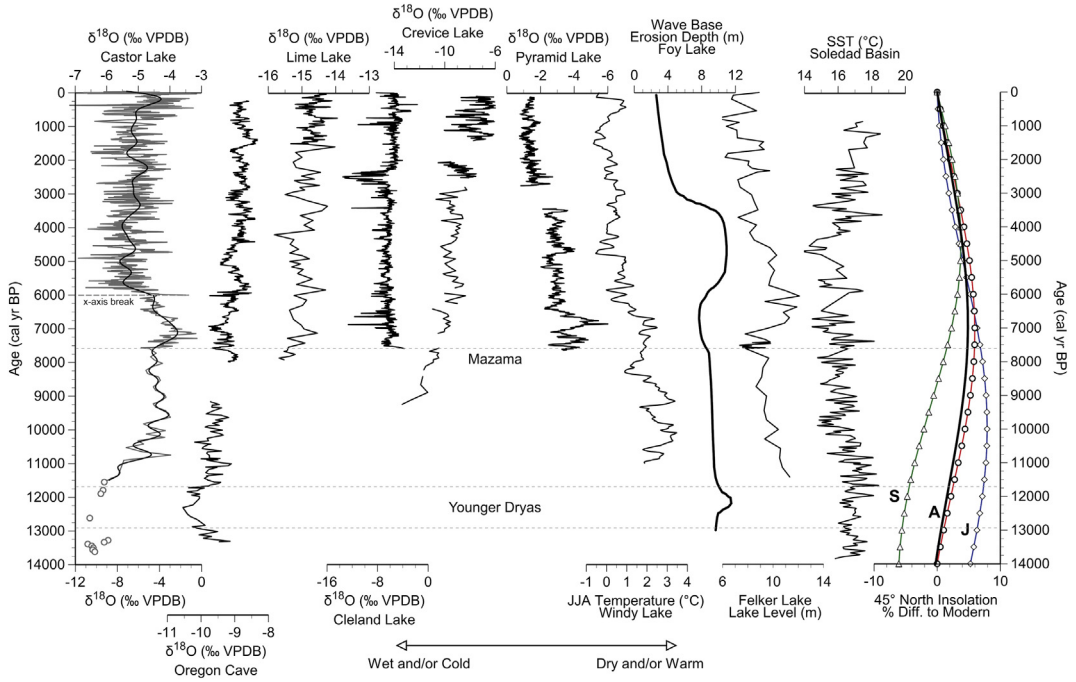

Fig. 12. Comparison of regional paleoclimate records from Castor Lake ($\delta^{18}O$) (black line: 500 year lowpass filter), OCNM speleothem ($\delta^{18}O$) (Ersek et al., 2012), Lime Lake ($\delta^{18}O$) (Steinman et al., 2016), Cleland Lake ($\delta^{18}O$) (Steinman et al., 2016), Crevice Lake ($\delta^{18}O$) (Whitlock et al., 2012), Pyramid Lake ($\delta^{18}O$) (Benson et al., 2002), Windy Lake (chironomid) (Chase et al., 2008), Foy Lake (sediment facies) (Shuman et al., 2009), Felker Lake (diatom) (Galloway et al., 2011), with eastern tropical Pacific SST (Mg/Ca in foraminifera) (Marchitto et al., 2010), and July (blue), August (red), September (green), and summer average (black) insolation at 45° North. The Foy Lake data are plotted as depth below modern level (e.g. lower levels occur in the middle Holocene). More negative $\delta^{18}O$ values in the Pyramid Lake data indicate drier conditions in response to decreased discharge from the Truckee River, which drains Lake Tahoe and has isotope values more positive than those of Pyramid Lake. (For interpretation of the references to colour in this figure legend, the reader is referred to the Web version of this article.)

scenario is that lake levels were substantially higher and that overflow occurred regularly, giving Castor Lake a more open-basin hydrologic configuration at this time. Reduced evapotranspiration resulting from undeveloped catchment vegetation and lower temperatures, and greater runoff due to the presence of nascent soils with low infiltration and water storage capacity are the most likely causes of higher lake levels. The sedimentological data, in particular the high residual MAR values, support this assertion.

4.4.2. Early/Middle Holocene climate/environmental variability (11,700 to 6200 yr BP)

The early Holocene $\delta^{18}O$ maximum in the Castor Lake record at 9630 (9110–10,100) yr BP is likely in part a result of higher summer insolation (Fig. 12), which produced higher temperatures and greater evaporation during the warm season. Additionally, atmospheric circulation in the early Holocene was substantially different from the modern configuration (Bartlein et al., 2014), and precipitation amounts were likely lower, due to the presence of the residual Laurentide and Cordilleran Ice Sheets (Dyke, 2004), which affected air mass trajectories and the seasonal distribution and amount of precipitation on a hemispheric scale. The isotopic composition of precipitation, as reflected by $\delta^{18}O$ values of the OCNM speleothem, increased by ~1.1‰ during the early Holocene and thus explains part of the much larger shift in $\delta^{18}O$ values in the Castor Lake record. A chironomid based climate reconstruction from Windy Lake, south-central British Columbia, supports the assertion that greater summer insolation produced warmer summer temperatures at this time (Chase et al., 2008). Consistent with the Castor Lake data, precipitation reconstructions from lakes on Vancouver Island indicate widespread dryness during the early Holocene between 11,000 and 7000 yr BP, with maximum aridity between 11,000 and 9000 yr BP (Brown et al., 2006). Analysis of sedimentary facies from Mahoney Lake in British Columbia (Lowe et al., 1997) and Foy Lake in Montana (Fig. 12) (Shuman et al., 2009) also suggest lower lake levels and dryness in the early Holocene. Multiproxy data from Big Lake, south central British Columbia, based on diatom, pigment, biogenic silica, and organic matter content analyses suggest moderate effective moisture prior to 8500 yr BP (Bennett et al., 2001). Gradually, through the early Holocene as the ice sheets retreated, a progression occurred toward the modern mode of atmospheric circulation characterized by the predominance of the Pacific westerlies (Bartlein et al., 1998; Thompson et al., 1993). This shift in atmospheric circulation likely produced gradually increasing but highly variable (and lower than present) precipitation amounts at Castor Lake between 9630 and 7600 yr BP, as reflected by the trend toward lower $\delta^{18}O$ values over this interval.

Climate model simulations and proxy data indicate a substantially different configuration of the Pacific ocean-atmosphere system during the middle Holocene (6000 yr BP) (Bartlein et al., 2014; Braconnot et al., 2007; Diffenbaugh and Sloan, 2004). By this time, the Cordilleran Ice Sheet was almost entirely gone, and the Laurentide Ice Sheet had retreated to northeastern North America (Dyke, 2004). Mean July to September insolation was substantially higher than at present, directly promoting drier conditions in the Pacific Northwest by increasing solar irradiance and surface temperatures during the warm season. Sea surface temperature records (Fig. 12) (Khider et al., 2014; Marchitto et al., 2010; Stott et al., 2007) and precipitation reconstructions from lake sedimentological analyses (Conroy et al., 2008; Moy et al., 2002) indicate a more La Niña like spatial pattern of tropical Pacific SSTs and possibly an attenuation of ENSO variance in the middle Holocene (Cobb et al., 2013; Koutavas

et al., 2006; Koutavas and Joanides, 2012). Terrestrial oxygen isotope records from the northeastern Pacific region (Anderson et al., 2005; Fisher et al., 2008), and biological productivity data from the Gulf of Alaska (Addison et al., 2012; Barron et al., 2009) indicate a weaker and more westerly position of the Aleutian Low and a more northerly position of the North Pacific high pressure system (Barron and Anderson, 2011). Several steady state climate model simulations forced by mid-Holocene boundary conditions support these inferences (Bartlein et al., 2014, 1998; Harrison et al., 2003; Hermann et al., 2018), reproducing an enhanced north Pacific high pressure system that blocks the westerly flow of moist air from the Pacific to the North American continental interior. Some mid-Holocene simulations indicate enhanced precipitation-evaporation balance seasonality in the Pacific Northwest, wherein the cold season was colder and wetter, and the warm season warmer and drier than at present (Steinman et al., 2016), although the magnitude of the change in the distribution of precipitation is small (Hermann et al., 2018) and spatially inconsistent among models (Hermann et al., 2018; Steinman et al., 2016).

The relatively rapid post-Mazama transitions in the Castor Lake $\delta^{18}O$ data are anomalous in comparison with most other records from the region, which indicate relatively gradual climate/environmental change in response to a post-glacial reconfiguration of the climate system (Chase et al., 2008; Hebda, 1995; Heinrichs et al., 2002; Shuman et al., 2009; Whitlock and Brunelle, 2006). For example, reconstructions of the isotopic composition of precipitation from $\delta^{18}O$ analysis of the OCNM speleothem and sediment from Lime Lake (~165 km to the east-northeast of Castor Lake) do not support the idea of a broad scale reorganization of atmospheric circulation during the post-Mazama lowstand period (Fig. 12) (Ersek et al., 2012; Steinman et al., 2016). Although $\delta^{18}O$ values in the Lime Lake data are slightly elevated at 7000 yr BP, the 8000 to 6000 yr BP time period in the OCNM and Lime Lake records is not anomalous in the context of long timescale trends in both datasets. Pollen data from Mud Lake and Bonaparte Meadows indicate that during the post-Mazama lowstand regional vegetation consisted principally of *Artemisia* with a lesser component of *Pinus* relative to the late Holocene, implying that climate was drier (Mack et al., 1979), but there is no evidence in the pollen records that suggests an abrupt shift in climate after the Mazama eruption. Several notable records, however, exhibit what are possibly direct responses to the ash deposition. Oxygen isotope data from Pyramid Lake (within the Mazama ashfall zone), for example, indicate that climate became drier relatively rapidly beginning at 7100 yr BP with the driest interval of the middle to late Holocene at ~6900 yr BP (Benson et al., 2002). Likewise, the chironomid head capsule record from Kilpoola Lake (54 km north of Castor Lake) indicates an abrupt increase in salinity just after the Mazama eruption that persisted for at least several centuries (Heinrichs et al., 1999), although dating limitations prevent any firm assessment of the lowstand duration. Heinrichs et al. (1999) attribute this increase in salinity to the weathering of the highly reactive andesitic/rhyodacitic ash and a subsequent increase in dissolved ion delivery to the lake. An alternative, mutually compatible possibility is that Kilpoola lake salinity increased after the Mazama eruption due to a decline in lake levels in addition to an increase in dissolved ion influx. The seismic reflection based lake-level reconstruction for Flathead Lake, northwestern Montana, provides additional evidence of potential lake hydrologic responses to the Mazama ashfall, indicating that levels dropped rapidly after the eruption and remained low for several millennia (Hofmann et al., 2006). Lastly, charophyte accumulation rate analysis of sediments from Dog Lake, southeastern British Columbia, indicate that following the Mazama eruption, lake levels declined for several centuries (Hallett and Hills, 2006), an inference consistent with the Castor $\delta^{18}O$ data.

In the Castor Lake record, average $\delta^{18}O$ values from the ~1000 years prior to the Mazama eruption are more positive than during any 1000 year period between the post-Mazama lowstand and 1000 yr BP (Fig. 9). This suggests that climate was drier before the Mazama eruption than later in the Holocene (prior to 1000 yr BP), and that the ash deposition likely produced lower lake levels than otherwise would have occurred. Pollen and diatom data from Big Lake, south-central British Columbia, suggest that the driest conditions of the Holocene occurred between 8500 and 7500 yr BP and were followed by a drier than present climate from 7500 to 6600 yr BP (Bennett et al., 2001). $\delta^{18}O$ and carbonate mineralogy data from Jones Lake, MT suggest that lake levels were lower (and evaporation rates greater) relative to present for as long as two millennia before and after the Mazama eruption and that the early Holocene (centered on ~9000 yr BP) was the driest interval of the record (Shapley et al., 2009). Markedly, the majority of pollen records suggest that in the Pacific Northwest, in comparison to the late Holocene, climate was warmer and drier during the early Holocene and at least warmer during most of the middle Holocene (Hebda, 1995; Whitlock, 1992; Whitlock and Brunelle, 2006), a pattern somewhat consistent with the Castor Lake $\delta^{18}O$ data, which indicate low lake levels from ~10,000 yr BP to 6190 yr BP. Several records contrast with the preponderance of evidence indicating a drier early/middle Holocene. These include the Crevice Lake, Montana, $\delta^{18}O$ record, which provides insight on precipitation during the cold season and indicates greater winter precipitation amounts between ~9000 and 6000 yr BP (Whitlock et al., 2012), and a diatom inferred lake-level reconstruction from Felker Lake, British Columbia, which indicates a lowstand centered on ~7200 yr BP followed by the highest lake levels of the Holocene at ~6000 yr BP (Fig. 12) (Galloway et al., 2011). Notably, lake sediment records from Vancouver Island, which are outside of the Mazama ash fall zone, exhibit no evidence for mid-Holocene drought and minimal changes in precipitation regimes after 7000 yr BP (Brown et al., 2006).

4.4.3. Middle/late Holocene climate/environmental variability (6200 yr BP to present)

The 6200 yr BP to present time period at Castor Lake was principally characterized by substantial multidecadal to multicentury time scale variability (Nelson et al., 2011), and a secular trend toward slightly drier conditions beginning ~5000 yr BP when the highest lake levels of the Holocene occurred, as evinced by the low $\delta^{18}O$ values in sediment from this time (Fig. 12). Many other proxy records exhibit substantial variability as well and, in some cases, results that are inconsistent with the Castor Lake data. Multiproxy data from Big Lake demonstrate higher effective moisture between ~6600 and 3600 yr BP and a trend toward drier conditions thereafter (Bennett et al., 2001). The middle through late Holocene data from Dog Lake are somewhat contradictory, suggesting dry, open forest from ~6000 to 4500 yr BP but simultaneously higher lake levels. This is followed by a transition to drier and more open vegetation with increased fire frequency between 2400 and 1200 yr BP (Hallett and Hills, 2006) and generally lower lake levels in the late Holocene. This disparity in the middle Holocene data from Dog Lake could potentially be the result of the seasonal sensitivity of the vegetation and lake-level proxies, with the former more responsive to climate during the warm season and the latter more strongly influenced by cold season climate (Steinman et al., 2016). A 6000 year varve sequence in the Saanich Inlet, British Columbia suggests wet conditions from 6000 to 3250 yr BP (Nederbragt and Thurow, 2001), a result that is somewhat consistent with both the Big Lake data (Bennett et al., 2001) and the record of depth changes at Felker Lake, which suggests declining lake levels between 6000 and ~2000 yr BP (Galloway et al., 2011). The Foy Lake level

reconstruction indicates the lowest levels of the Holocene between ~5500 and 3500 yr BP, in direct contrast to several of the aforementioned datasets, but consistent with many others (see Shuman et al., 2009 for additional detail). Interestingly, lake-level records from Lake of the Woods, Wyoming, and Emerald Lake, Colorado, indicate a rapid increase in effective moisture at ~5700 yr BP (Shuman et al., 2014), which is consistent with the timing of a transition to more negative $\delta^{18}O$ values and higher lake levels at Castor Lake. Directly comparable $\delta^{18}O$ records from Cleland Lake (Steinman et al., 2016) and Crevice Lake (Whitlock et al., 2012) are somewhat consistent with the Castor Lake $\delta^{18}O$ data, demonstrating greater $\delta^{18}O$ values in the late Holocene relative to ~6000 years before present. The inconsistency among some middle Holocene climate records from the Pacific Northwest is likely a result of several factors: namely, differences in the seasonal sensitivities of proxies, climate shifts that involve conflicting seasonal responses (e.g. enhanced seasonality of temperature and/or precipitation), and spatial heterogeneity in climate change due to, for example, complex topography and orographic effects on atmospheric circulation.

5. Conclusions

The multi-proxy sediment record from Castor Lake and facies changes in sediment from Scanlon Lake provide a late Quaternary perspective on hydroclimate and ecosystem variability in north-central Washington. In the Castor Lake sediment, marked changes in the mass accumulation rate of organic carbon, nitrogen, residual minerogenic content, and the TOC/TN ratio suggest a lake system response to the Younger Dryas cold reversal characterized by terrestrial vegetation declines, catchment destabilization, and greater erosion in response to a colder climate. High $\delta^{18}O$ values at 9630 yr BP indicate lower lake levels and a dry early Holocene. The middle Holocene at Castor Lake and Scanlon Lake was marked by a transition to a pronounced lowstand from ~7300 to 7100 yr BP, subsequent to the Mazama eruption and tephra deposition. $\delta^{18}O$ values in the Castor Lake sediment increase to the highest levels of the Holocene within several centuries of the eruption and remain high until 6190 yr BP, approximately consistent with a commensurate shift from laminated to mottled sediment facies indicative of very low lake levels. Lithological changes in the Scanlon Lake record shift from laminated to mixed sediments containing magnesium carbonates, suggest a similar pattern of lake-level change. The relatively rapid onset, and prolonged duration of extremely low lake levels at both Castor Lake and Scanlon Lake following Mazama eruption indicate that catchment hydrology was likely altered by the deposition of volcanic ash and its weathering to form clays, which increased catchment water retention and losses via evapotranspiration, and thereby reduced runoff. The lack of a post-Mazama eruption response in the OCNM and Lime Lake $\delta^{18}O$ records indicates that a large-scale shift in atmospheric circulation did not occur and is therefore consistent with the notion that the eruption and ash deposition was at least partially responsible for the change in lake level.

The Castor Lake multi-proxy data exhibit considerable multi-decadal to multi-century scale variability and a gradual trend toward slightly drier conditions over the last 6000 years, a temporal pattern that is consistent with some, but not all, records from the greater Pacific Northwest region. This disparity could be a result of seasonal sensitivities of the different proxies and/or spatial heterogeneity in climate change. Most notably, $\delta^{18}O$ data from southeastern British Columbia (Steinman et al., 2016) and southwestern Montana (Whitlock et al., 2012) suggest that cold season precipitation amounts in the late Holocene were lower than during the middle Holocene around 5000 years BP, a result that is consistent with the Castor Lake $\delta^{18}O$ data. The development of new lake sediment based paleorecords may help to reconcile these discrepancies and will provide further insight into the spatial and temporal pattern of climate change in the Pacific Northwest during the Holocene.

The relatively rapid and sustained decline in lake levels at Castor Lake and Scanlon Lake following the Mazama climactic eruption underscores the possibility that cataclysmic volcanic eruptions that deposit thick ash sequences on a regional scale can fundamentally alter catchment hydrologic characteristics for centuries following the eruption, and thereby confound lake sediment records of climate change in certain settings. If such an eruption were to occur in the future, changes in lake hydrology and ecosystem dynamics, river discharge, and agriculture would likely be far more spatially extensive and of greater magnitude and duration than any experienced in recent history in response to either droughts or smaller volcanic eruptions.

Acknowledgements

B.A.S acknowledges support from the U.S. National Science Foundation: (AGS-1137750, EAR-1447048). B.P.F. acknowledges U.S. National Science Foundation grants: (AGS 0402060, EPS-0814387).

Appendix A. Supplementary data

Supplementary data related to this article can be found at https://doi.org/10.1016/j.quascirev.2018.09.018.

References

Abbott, M.B., Binford, M.W., Brenner, M., Kelts, K.R., 1997. A 3500 14C yr high-resolution record of water-level changes in lake Titicaca, Bolivia/Peru. Quat. Res. 47, 169–180. https://doi.org/10.1006/qres.1997.1881.

Abbott, M.B., Finney, B.P., Edwards, M.E., Kelts, K.R., 2000. lake-level reconstruction and paleohydrology of Birch lake, central Alaska, based on seismic reflection profiles and core Transects. Quat. Res. 53, 154–166. https://doi.org/10.1006/qres.1999.2112.

Abbott, M.B., Stafford Jr., T.W., 1996. Radiocarbon geochemistry of modern and ancient Arctic lake systems, Baffin Island, Canada. Quat. Res. 45, 300–311. https://doi.org/10.1006/qres.1996.0031.

Addison, J.A., Finney, B.P., Dean, W.E., Davies, M.H., Mix, A.C., Stoner, J.S., Jaeger, J.M., 2012. Productivity and sedimentary δ15N variability for the last 17,000 years along the northern Gulf of Alaska continental slope. Paleoceanography 27. https://doi.org/10.1029/2011PA002161.

Andersen, K.K., Azuma, N., Barnola, J.-M., Bigler, M., Biscaye, P., Caillon, N., Chappellaz, J., Clausen, H.B., Dahl-Jensen, D., Fischer, H., Flückiger, J., Fritzsche, D., Fujii, Y., Goto-Azuma, K., Grønvold, K., Gundestrup, N.S., Hansson, M., Huber, C., Hvidberg, C.S., Johnsen, S.J., Jonsell, U., Jouzel, J., Kipfstuhl, S., Landais, a, Leuenberger, M., Lorrain, R., Masson-Delmotte, V., Miller, H., Motoyama, H., Narita, H., Popp, T., Rasmussen, S.O., Raynaud, D., Rothlisberger, R., Ruth, U., Samyn, D., Schwander, J., Shoji, H., Siggard-Andersen, M.-L., Steffensen, J.P., Stocker, T., Sveinbjörnsdóttir, a E., Svensson, a, Takata, M., Tison, J.-L., Thorsteinsson, T., Watanabe, O., Wilhelms, F., White, J.W.C., 2004. High-resolution record of Northern Hemisphere climate extending into the last interglacial period. Nature 431, 147–151. https://doi.org/10.1038/nature02805.

Anderson, L., Abbott, M.B., Finney, B.P., Burns, S.J., 2005. Regional atmospheric circulation change in the North Pacific during the Holocene inferred from lacustrine carbonate oxygen isotopes, Yukon Territory, Canada. Quat. Res. 64, 21–35. https://doi.org/10.1016/j.yqres.2005.03.005.

Anderson, L., Berkelhammer, M., Barron, J.A., Steinman, B.A., Finney, B.P., Abbott, M.B., 2016. Lake oxygen isotopes as recorders of North American Rocky Mountain hydroclimate: holocene patterns and variability at multi-decadal to millennial time scales. Global Planet. Change 137, 131–148. https://doi.org/10.1016/j.gloplacha.2015.12.021.

Antos, J.A., Zobel, D.B., 1986a. Recovery of forest understories buried by tephra from Mount St. Helens. Vegetatio 64, 103–111. https://doi.org/10.1007/BF00044786.

Antos, J.A., Zobel, D.B., 1986b. Seedling establishment in forests affected by tephra from Mount St. Helens. Am. J. Bot. 73, 495–499.

Araguás-Araguás, L., Froehlich, K., Rozanski, K., 2000. Deuterium and oxygen-18 isotope composition of precipitation and atmospheric moisture. Hydrol. Process. 14, 1341–1355. https://doi.org/10.1002/1099-1085(20000615)14:8<1341::AID-HYP983>3.0.CO;2-Z.

Barnett, T., Malone, R., Pennell, W., Stammer, D., Semtner, B., Washington, W., 2004.

The effects of climate change on water resources in the west: introduction and overview. Climatic Change 62, 1–11. https://doi.org/10.1023/B:CLIM.0000013695.21726.b8.
Barron, J.A., Anderson, L., 2011. Enhanced late holocene ENSO/PDO expression along the margins of the eastern North pacific. Quat. Int. 235, 3–12. https://doi.org/10.1016/j.quaint.2010.02.026.
Barron, J.A., Bukry, D., Dean, W.E., Addison, J.A., Finney, B., 2009. Paleoceanography of the Gulf of Alaska during the past 15,000 years: results from diatoms, silicoflagellates, and geochemistry. Mar. Micropaleontol. 72, 176–195. https://doi.org/10.1016/j.marmicro.2009.04.006.
Bartlein, P.J., Anderson, K.H., Anderson, P.M., Edwards, M.E., Mock, C.J., Thompson, R.S., Webb, R.S., Webb, T., Whitlock, C., 1998. Paleoclimate simulations for North America over the past 21,000 years: features of the simulated climate and comparisons with paleoenvironmental data. Quat. Sci. Rev. 17, 549–585. https://doi.org/10.1016/S0277-3791(98)00012-2.
Bartlein, P.J., Hostetler, S.W., Alder, J.R., 2014. Paleoclimate. In: Ohring, G. (Ed.), Climate Change in North America, Regional Climate Studies. Springer International Publishing, Cham Heidelberg New York Dordrecht London, pp. 1–51. https://doi.org/10.1007/978-3-319-03768-4.
Bennett, J.R., Cumming, B.F., Leavitt, P.R., Chiu, M., Smol, J.P., Szeicz, J., 2001. Diatom, pollen, and chemical evidence of postglacial climatic change at Big Lake, south-central British Columbia, Canada. Quat. Res. 55, 332–343. https://doi.org/10.1006/qres.2001.2227.
Benson, L., Kashgarian, M., Rye, R., Lund, S., Paillet, F., Smoot, J., Kester, C., Mensing, S., Meko, D., Lindström, S., 2002. Holocene multidecadal and multicentennial droughts affecting Northern California and Nevada. Quat. Sci. Rev. 21, 659–682. https://doi.org/10.1016/S0277-3791(01)00048-8.
Benson, L., Paillet, F., 2002. HIBAL: a hydrologic-isotopic-balance model for application to paleolake systems. Quat. Sci. Rev. 21, 1521–1539. https://doi.org/10.1016/S0277-3791(01)00094-4.
Bowen, G.J., Revenaugh, J., 2003. Interpolating the isotopic composition of modern meteoric precipitation. Water Resour. Res. 39, 1299. https://doi.org/10.1029/2003WR002086.
Braconnot, P., Otto-Bliesner, B., Harrison, S., Joussaume, S., Peterchmitt, J.-Y., Abe-Ouchi, A., Crucifix, M., Driesschaert, E., Fichefet, T., Hewitt, C.D., Kageyama, M., Kitoh, A., Laîné, A., Loutre, M.-F., Marti, O., Merkel, U., Ramstein, G., Valdes, P., Weber, S.L., Yu, Y., Zhao, Y., 2007. Results of PMIP2 coupled simulations of the Mid-Holocene and Last Glacial Maximum – Part 1: experiments and large-scale features. Clim. Past 3, 261–277. https://doi.org/10.5194/cp-3-261-2007.
Briggs, C.A.D., Busacca, A.J., McDaniel, P.A., 2006. Pedogenic processes and soil-landscape relationships in north cascades national park, Washington. Geoderma 137, 192–204. https://doi.org/10.1016/j.geoderma.2006.08.015.
Brown, K.J., Fitton, R.J., Schoups, G., Allen, G.B., Wahl, K.A., Hebda, R.J., 2006. Holocene precipitation in the coastal temperate rainforest complex of southern British Columbia, Canada. Quat. Sci. Rev. 25, 2762–2779. https://doi.org/10.1016/j.quascirev.2006.02.020.
Bryson, R.A., Hare, F.K., 1974. The climates of north America. In: Climates of North America, pp. 1–47.
Chase, M., Bleskie, C., Walker, I.R., Gavin, D.G., Hu, F.S., 2008. Midge-inferred holocene summer temperatures in southeastern British Columbia, Canada. Palaeogeogr. Palaeoclimatol. Palaeoecol. 257, 244–259. https://doi.org/10.1016/j.palaeo.2007.10.020.
Clague, J.J., James, T.S., 2002. History and isostatic effects of the last ice sheet in southern British Columbia. Quat. Sci. Rev. 21, 71–87. https://doi.org/10.1016/S0277-3791(01)00070-1.
Cobb, K.M., Westphal, N., Sayani, H.R., Watson, J.T., Di Lorenzo, E., Cheng, H., Edwards, R.L., Charles, C.D., 2013. Highly variable el niño-southern oscillation throughout the holocene. Science 339, 67–70. https://doi.org/10.1126/science.1228246.
Conroy, J.L., Overpeck, J.T., Cole, J.E., Shanahan, T.M., Steinitz-Kannan, M., 2008. Holocene changes in eastern tropical Pacific climate inferred from a Galápagos lake sediment record. Quat. Sci. Rev. 27, 1166–1180. https://doi.org/10.1016/j.quascirev.2008.02.015.
Craig, H., Gordon, L., 1965. Deuterium and oxygen 18 variation in the ocean and marine atmosphere. In: E., T (Ed.), Stable Isotopes in Oceanographic Studies and Palaeotemperatures. Consiglio Nazionale della Ricerca, Pisa, Italy, pp. 9–130.
Dean, W.E.J., 1974. Determination of carbonate and organic matter in calcareous sediments and sedimentary rocks by loss on ignition: comparison with other methods. J. Sediment. Petrol. 44, 242–248. https://doi.org/10.1306/74D729D2-2B21-11D7-8648000102C1865D.
Diefendorf, A.F., Patterson, W.P., Holmden, C., Mullins, H.T., 2008. Carbon isotopes of marl and lake sediment organic matter reflect terrestrial landscape change during the late Glacial and early Holocene (16,800 to 5,540 cal yr B.P.): a multiproxy study of lacustrine sediments at Lough Inchiquin, western Ireland. J. Paleolimnol. 39, 101–115. https://doi.org/10.1007/s10933-007-9099-9.
Diffenbaugh, N.S., Sloan, L.C., 2004. Mid-Holocene orbital forcing of regional-scale climate: a case study of western north America using a high-resolution RCM. J. Clim. 17, 2927–2937. https://doi.org/10.1175/1520-0442(2004)017<2927:MOFORC>2.0.CO;2.
Dyke, A.S., 2004. An outline of North American deglaciation with emphasis on central and northern Canada. Dev. Quat. Sci. 2, 373–424. https://doi.org/10.1016/S1571-0866(04)80209-4.
Ersek, V., Clark, P.U., Mix, A.C., Cheng, H., Edwards, R.L., 2012. Holocene winter climate variability in mid-latitude western North America. Nat. Commun. 3, 1219. https://doi.org/10.1038/ncomms2222.
Finkenbinder, M.S., Abbott, M.B., Edwards, M.E., Langdon, C.T., Steinman, B.A., Finney, B.P., 2014. A 31,000 year record of paleoenvironmental and lake-level change from Harding Lake, Alaska, USA. Quat. Sci. Rev. 87, 98–113. https://doi.org/10.1016/j.quascirev.2014.01.005.
Finney, B.P., Bigelow, N.H., Barber, V.A., Edwards, M.E., 2012. Holocene climate change and carbon cycling in a groundwater-fed, boreal forest lake: Dune Lake, Alaska. J. Paleolimnol. 48, 43–54. https://doi.org/10.1007/s10933-012-9617-2.
Finney, B.P., Gregory-Eaves, I., Sweetman, J., Douglas, M.S., Smol, J.P., 2000. Impacts of climatic change and fishing on Pacific salmon abundance over the past 300 years. Science 84 290, 795–799. https://doi.org/10.1126/science.290.5492.795.
Fisher, D., Osterberg, E., Dyke, A., Dahl-Jensen, D., Demuth, M., Zdanowicz, C., Bourgeois, J., Koerner, R.M., Mayewski, P., Wake, C., Kreutz, K., Steig, E., Zheng, J., Yalcin, K., Goto-Azuma, K., Luckman, B., Rupper, S., 2008. The Mt Logan Holocene – late Wisconsinan isotope record: tropical Pacific – Yukon connections. Holocene 18, 667–677. https://doi.org/10.1177/0959683608092236.
Foit Jr., F.F., Mehringer Jr., P.J., Sheppard, J.C., 1993. Age, distribution, and stratigraphy of Glacier Peak tephra in eastern Washington and western Montana, United States. Can. J. Earth Sci. 30, 535–552. https://doi.org/10.1139/e93-042.
Galloway, J.M., Lenny, A.M., Cumming, B.F., 2011. Hydrological change in the central interior of British Columbia, Canada: diatom and pollen evidence of millennial-to-centennial scale change over the Holocene. J. Paleolimnol. 45, 183–197. https://doi.org/10.1007/s10933-010-9490-9.
Gat, J.R., 1996. Oxygen and hydrogen isotopes in the hydrologic Cycle. Annu. Rev. Earth Planet Sci. 24, 225–262. https://doi.org/10.1146/annurev.earth.24.1.225.
Geist, J.M., Strickler, G.S., 1978. Physical and Chemical Properties of Some Blue Mountain Soils in the Northeastern Oregon. Pacific Northwest Forest and Range Experiment Station, U.S. Dept. of Agriculture, Portland, OR.
Hallett, D.J., Hills, L.V., 2006. Holocene vegetation dynamics, fire history, lake level and climate change in the Kootenay Valley, southeastern British Columbia, Canada. J. Paleolimnol. 35, 351–371. https://doi.org/10.1007/s10933-005-1335-6.
Hallett, D.J., Hills, L.V., Clague, J.J., 1997. New accelerator mass spectrometry radiocarbon ages for the Mazama tephra layer from Kootenay National Park, British Columbia, Canada. Can. J. Earth Sci. 34, 1202–1209. https://doi.org/10.1139/e17-096.
Hammarlund, D., Aravena, R., Barnekow, L., Buchardt, B., Possnert, G., 1997. Multicomponent carbon isotope evidence of early Holocene environmental change and carbon-flow pathways from a hard-water lake in northern Sweden. J. Paleolimnol. 18, 219–233. https://doi.org/10.1023/A:1007953614927.
Harrison, S., Kutzbach, J., Liu, Z., Bartlein, P., 2003. Mid-Holocene climates of the Americas: a dynamical response to changed seasonality. Clim. Dynam. 20, 663–688. https://doi.org/10.1007/s00382-002-0300-6.
Haslett, J., Parnell, A., 2008. A simple monotone process with application to radiocarbon-dated depth chronologies. J. R. Stat. Soc. Ser. C Appl. Stat. 57, 399–418. https://doi.org/10.1111/j.1467-9876.2008.00623.x.
Hebda, R.J., 1995. British Columbia vegetation and climate history with focus on 6 ka BP. Géogr. Phys. Quaternaire 49, 66–79. https://doi.org/10.7202/033030ar.
Heine, J.T., 1998. Extent, timing, and climatic implications of glacier advances Mount Rainier, Washington, U.S.A., at the Pleistocene/Holocene transition. Quat. Sci. Rev. 17, 1139–1148. https://doi.org/10.1016/S0277-3791(97)00077-2.
Heinrichs, M.L., Hebda, R.J., Walker, I.R., Palmer, S.L., 2002. Postglacial paleoecology and inferred paleoclimate in the Engelmann spruce-subalpine fir forest of south-central British Columbia, Canada. Palaeogeogr. Palaeoclimatol. Palaeoecol. 184, 347–369. https://doi.org/10.1016/S0031-0182(02)00274-2.
Heinrichs, M.L., Walker, I.R., Mathewes, R.W., Hebda, R.J., 1999. Holocene chironomid-inferred salinity and paleovegetation reconstruction from Kilpoola Lake, British Columbia. Géogr. Phys. Quaternaire 53, 211–221. https://doi.org/10.7202/004878ar.
Henderson, A.K., Shuman, B.N., 2009. Hydrogen and oxygen isotopic compositions of lake water in the western United States. Geol. Soc. Am. Bull. 121, 1179–1189. https://doi.org/10.1130/B26441.1.
Hermann, N.W., Oster, J.L., Ibarra, D.E., 2018. Spatial patterns and driving mechanisms of mid-Holocene hydroclimate in western North America. J. Quat. Sci. 33, 421–434. https://doi.org/10.1002/jqs.3023.
Hoblitt, R., Miller, C., Scott, W., 1987. Volcanic Hazards with Regard to Siting Nuclear-power Plants in the Pacific Northwest. Vancouver, WA.
Hodell, D.A., Schelske, C.L., Fahnenstiel, G.L., Robbins, L.L., 1998. Biologically induced calcite and its isotopic composition in Lake Ontario. Limnol. Oceanogr. 43, 187–199. https://doi.org/10.4319/lo.1998.43.2.0187.
Hofmann, M.H., Hendrix, M.S., Moore, J.N., Sperazza, M., 2006. Late pleistocene and holocene depositional history of sediments in Flathead Lake, Montana: Evidence from high-resolution seismic reflection interpretation. Sediment. Geol. 184, 111–131. https://doi.org/10.1016/j.sedgeo.2005.09.019.
Horton, T.W., Defliese, W.F., Tripati, A.K., Oze, C., 2016. Evaporation induced 18O and 13C enrichment in lake systems: A global perspective on hydrologic balance effects. Quat. Sci. Rev. 131, 365–379. https://doi.org/10.1016/j.quascirev.2015.06.030.
Jones, M.D., Imbers, J., 2010. Modeling Mediterranean lake isotope variability. Global Planet. Change 71, 193–200. https://doi.org/10.1016/j.gloplacha.2009.10.001.
Jones, M.D., Roberts, C.N., Leng, M.J., Türkeş, M., 2006. A high-resolution late Holocene lake isotope record from Turkey and links to North Atlantic and monsoon climate. Geology 34, 361. https://doi.org/10.1130/G22407.1.
Jones, M.D., Roberts, N.C., 2008. Interpreting lake isotope records of Holocene environmental change in the Eastern Mediterranean. Quat. Int. 181, 32–38. https://doi.org/10.1016/j.quaint.2007.01.012.

Kelts, K., Talbot, M., 1990. Lacustrine Carbonates as Geochemical Archives of Environmental Change and Biotic/Abiotic Interactions. Springer, Berlin, Heidelberg, pp. 288–315. https://doi.org/10.1007/978-3-642-84077-7_15.
Khider, D., Jackson, C.S., Stott, L.D., 2014. Assessing millennial-scale variability during the Holocene: A perspective from the western tropical Pacific. Paleoceanography 29, 143–159. https://doi.org/10.1002/2013PA002534.
Kirby, M.E., Zimmerman, S.R.H., Patterson, W.P., Rivera, J.J., 2012. A 9170-year record of decadal-to-multi-centennial scale pluvial episodes from the coastal Southwest United States: A role for atmospheric rivers? Quat. Sci. Rev. 46, 57–65. https://doi.org/10.1016/j.quascirev.2012.05.008.
Koutavas, A., DeMenocal, P.B., Olive, G.C., Lynch-Stieglitz, J., 2006. Mid-Holocene El Niño–Southern Oscillation (ENSO) attenuation revealed by individual foraminifera in eastern tropical Pacific sediments. Geology 34, 993–996. https://doi.org/10.1130/G22810A.1.
Koutavas, A., Joanides, S., 2012. El Niño-Southern Oscillation extrema in the Holocene and Last Glacial Maximum. Paleoceanography 27. https://doi.org/10.1029/2012PA002378 n/a-n/a.
Kuehn, S.C., Froese, D.G., Carrara, P.E., Foit, F.F., Pearce, N.J.G., Rotheisler, P., 2009. Major- and trace-element characterization, expanded distribution, and a new chronology for the latest Pleistocene Glacier Peak tephras in western North America. Quat. Res. 71, 201–216. https://doi.org/10.1016/j.yqres.2008.11.003.
Leavesley, G.H., Lusby, G.C., Lichty, R.W., 1989. Infiltration and erosion characteristics of selected tephra deposits from the 1980 eruption of Mount St. Helens, Washington, USA. Hydrol. Sci. J. 34, 339–353. https://doi.org/10.1080/02626668909491338.
Leng, M.J., Marshall, J.D., 2004. Palaeoclimate interpretation of stable isotope data from lake sediment archives. Quat. Sci. Rev. 23, 811–831. https://doi.org/10.1016/j.quascirev.2003.06.012.
Li, H.C., Ku, T.L., 1997. δ13C-δ18O covariance as a paleohydrological indicator for closed-basin lakes. Palaeogeogr. Palaeoclimatol. Palaeoecol. 133, 69–80. https://doi.org/10.1016/S0031-0182(96)00153-8.
Lohne, O.S., Mangerud, J., Birks, H.H., 2014. IntCal13 calibrated ages of the Vedde and Saksunarvatn ashes and the Younger Dryas boundaries from Kråkenes, western Norway. J. Quat. Sci. 29, 506–507. https://doi.org/10.1002/jqs.2722.
Lohne, O.S., Mangerud, J., Birks, H.H., 2013. Precise 14C ages of the Vedde and Saksunarvatn ashes and the Younger Dryas boundaries from western Norway and their comparison with the Greenland Ice Core (GICC05) chronology. J. Quat. Sci. 28, 490–500. https://doi.org/10.1002/jqs.2640.
Lowe, D.J., Green, J.D., Northcote, T.G., Hall, K.J., 1997. Holocene Fluctuations of a Meromictic Lake in Southern British Columbia. Quat. Res. 48, 100–113. https://doi.org/10.1006/qres.1997.1905.
Mack, R.N., Rutter, N.W., Valastro, S., 1979. Holocene vegetation history of the Okanogan Valley, Washington. Quat. Res. 12, 212–225. https://doi.org/10.1016/0033-5894(79)90058-9.
Major, J.J., Yamakoshi, T., 2005. Decadal-scale change of infiltration characteristics of a tephra-mantled hillslope at Mount St Helens, Washington. Hydrol. Process. 19, 3621–3630. https://doi.org/10.1002/hyp.5863.
Mann, M.E., 2008. Smoothing of climate time series revisited. Geophys. Res. Lett. 35, L16708. https://doi.org/10.1029/2008GL034716.
Marchitto, T.M., Muscheler, R., Ortiz, J.D., Carriquiry, J.D., van Geen, A., 2010. Dynamical response of the tropical Pacific Ocean to solar forcing during the early Holocene. Science 330, 1378–1381. https://doi.org/10.1126/science.1194887.
McDaniel, P.A., Wilson, M.A., Burt, R., Lammers, D., Thorson, T.D., McGrath, C.L., Peterson, N., 2005. Andic Soils of the Inland Pacific Northwest, USA: Properties and Ecological Significance. Soil Sci. 170, 300–311.
McDaniel, P., Wilson, M., 2007. Physical and Chemical Characteristics of Ash-influenced Soils of Inland Northwest Forests, pp. 31–45.
Meurisse, R.T., Robbie, W.A., Niehoff, J., Ford, G., 1991. Dominant soil formation processes and properties in western-montane forest types and landscapes – Some implications for productivity and management. In: Management and Productivity of Western-montane Forest Soils. US Forest Service Intermountain Research Station, Ogden, UT, Boise, ID, pp. 7–19.
Meyers, P.A., Teranes, J.L., 2001. Sediment organic matter. Physical and Geochemical Methods. In: Tracking Environmental Change Using Lake Sediments, vol. 2, pp. 239–269. https://doi.org/10.1897/1551-5028(1999)018<0231:SOMCAA>2.3.CO;2.
Miller, D.E., Gardner, W.H., 1962. Water Infiltration Into Stratified Soil. Soil Sci. Soc. Am. J. 26, 115–119. https://doi.org/10.2136/sssaj1962.03615995002600020007x.
Mote, P.W., Parson, E.A., Hamlet, A.F., Keeton, W.S., Lettenmaier, D., Mantua, N., Miles, E.L., Peterson, D.W., Peterson, D.L., Slaughter, R., Snover, A.K., 2003. Preparing for Climatic Change: The Water, Salmon, and Forests of the Pacific Northwest. Climatic Change 61, 45–88. https://doi.org/10.1023/A:1026302914358.
Moy, C.M., Seltzer, G.O., Rodbell, D.T., Anderson, D.M., 2002. Variability of El Niño/Southern Oscillation activity at millennial timescales during the Holocene epoch. Nature 420, 162–165. https://doi.org/10.1038/nature01194.
Müller, G., Irion, G., Fürstner, U., 1972. Formation and diagenesis of inorganic Ca-Mg carbonates in the lacustrine environment. Naturwissenschaften 59, 158–164. https://doi.org/10.1007/BF00637354.
Mullineaux, D.R., 1986. Summary of pre-1980 tephra-fall deposits erupted from Mount St. Helens, Washington State, USA. Bull. Volcanol. 48, 17–26. https://doi.org/10.1007/BF01073510.
Muschitiello, F., Wohlfarth, B., 2015. Time-transgressive environmental shifts across Northern Europe at the onset of the Younger Dryas. Quat. Sci. Rev. 109, 49–56. https://doi.org/10.1016/j.quascirev.2014.11.015.
NCSS, 2006. Custom Soil Resource Report for Okanogan County Area, Washington.
Neall, V.E., 2006. Volcanic Soils. In: Verheye, W. (Ed.), Land Use and Land Cover, Encyclopaedia of Life Support Systems (EOLSS). EOLSS Publishers with UNESCO, Oxford, U.K., pp. 1–24
Nederbragt, A.J., Thurow, J.W., 2001. A 6000 yr varve record of Holocene climate in Saanich Inlet, British Columbia, from digital sediment colour analysis of ODP Leg 169s cores. Mar. Geol. 174, 95–110. https://doi.org/10.1016/S0025-3227(00)00144-4.
Nelson, D.B., 2004. Holocene Paleoenvironmental History from Stable Isotopes in Lake Sediment, North-Central Washington State. Pittsburgh.
Nelson, D.B., Abbott, M.B., Steinman, B., Polissar, P.J., Stansell, N.D., Ortiz, J.D., Rosenmeier, M.F., Finney, B.P., Riedel, J., 2011. Drought variability in the Pacific Northwest from a 6,000-yr lake sediment record. Proc. Natl. Acad. Sci. U. S. A 108, 3870–3875. https://doi.org/10.1073/pnas.1009194108.
Ogawa, Y., Daimaru, H., Shimizu, A., 2007. Experimental study of post-eruption overland flow and sediment load from slopes overlain by pyroclastic-flow deposits, Unzen volcano, Japan. Géomorphol. Relief, Process. Environ. 237–246. https://doi.org/10.4000/geomorphologie.3962.
Parnell, A.C., Buck, C.E., Doan, T.K., 2011. A review of statistical chronology models for high-resolution, proxy-based Holocene palaeoenvironmental reconstruction. Quat. Sci. Rev. 30, 2948–2960. https://doi.org/10.1016/j.quascirev.2011.07.024.
Parnell, A.C., Haslett, J., Allen, J.R.M., Buck, C.E., Huntley, B., 2008. A flexible approach to assessing synchroneity of past events using Bayesian reconstructions of sedimentation history. Quat. Sci. Rev. 27, 1872–1885. https://doi.org/10.1016/j.quascirev.2008.07.009.
Pfitsch, W.A., Bliss, L.C., 1988. Recovery of net primary production in subalpine meadows of Mount St. Helens following the 1980 eruption. Can. J. Bot. 66, 989–997. https://doi.org/10.1139/b88-142.
Pierson, T.C., Major, J.J., 2014. Hydrogeomorphic Effects of Explosive Volcanic Eruptions on Drainage Basins*. Annu. Rev. Earth Planet Sci. 42, 469–507. https://doi.org/10.1146/annurev-earth-060313-054913.
Ping, C.L., 2000. Volcanic soils. In: Sigurdsson, H. (Ed.), Encyclopedia of Volcanoes. Academic Press, San Diego, CA, pp. 1259–1270.
Rasmussen, S.O., Andersen, K.K., Svensson, A.M., Steffensen, J.P., Vinther, B.M., Clausen, H.B., Siggaard-Andersen, M.L., Johnsen, S.J., Larsen, L.B., Dahl-Jensen, D., Bigler, M., Röthlisberger, R., Fischer, H., Goto-Azuma, K., Hansson, M.E., Ruth, U., 2006. A new Greenland ice core chronology for the last glacial termination. J. Geophys. Res. Atmos. 111 https://doi.org/10.1029/2005JD006079.
Reimer, P., 2013. IntCal13 and Marine13 Radiocarbon Age Calibration Curves 0–50,000 Years cal BP. Radiocarbon 55, 1869–1887. https://doi.org/10.2458/azu_js_rc.55.16947.
Rinehart, C.D., Fox, K.F., 1976. Bedrock Geology of the Conconully Quadrangle, Okanogan County, Washington - Charles Dean Rinehart, Kenneth F. Fox. Geol. Surv. Bull. 1402.
Roberts, N., Reed, J.M., Leng, M.J., Kuzucuoğlu, C., Fontugne, M., Bertaux, J., Woldring, H., Bottema, S., Black, S., Hunt, E., Karabiyikoğlu, M., 2001. The tempo of Holocene climatic change in the eastern Mediterranean region: new high-resolution crater-lake sediment data from central Turkey. Holocene 11, 721–736. https://doi.org/10.1191/09596830195744.
Shapley, M.D., Ito, E., Donovan, J.J., 2009. Lateglacial and Holocene hydroclimate inferred from a groundwater flow-through lake, Northern Rocky Mountains, USA. Holocene. https://doi.org/10.1177/0959683609104029.
Shapley, M.D., Ito, E., Donovan, J.J., 2008. Isotopic evolution and climate paleorecords: Modeling boundary effects in groundwater-dominated lakes. J. Paleolimnol. 39, 17–33. https://doi.org/10.1007/s10933-007-9092-3.
Shapley, M.D., Ito, E., Donovan, J.J., 2005. Authigenic calcium carbonate flux in groundwater-controlled lakes: Implications for lacustrine paleoclimate records. Geochem. Cosmochim. Acta 69, 2517–2533. https://doi.org/10.1016/j.gca.2004.12.001.
Shuman, B., Bravo, J., Kaye, J., Lynch, J. a, Newby, P., Webb III, T., 2001. Late Quaternary Water-Level Variations and Vegetation History at Crooked Pond, Southeastern Massachusetts. Quat. Res. 56, 401–410. https://doi.org/10.1006/qres.2001.2273.
Shuman, B., Henderson, A.K., Colman, S.M., Stone, J.R., Fritz, S.C., Stevens, L.R., Power, M.J., Whitlock, C., 2009. Holocene lake-level trends in the Rocky Mountains. U.S.A. Quat. Sci. Rev. 28, 1861–1879. https://doi.org/10.1016/j.quascirev.2009.03.003.
Shuman, B., Pribyl, P., Minckley, T.A., Shinker, J.J., 2010. Rapid hydrologic shifts and prolonged droughts in Rocky Mountain headwaters during the Holocene. Geophys. Res. Lett. 37 https://doi.org/10.1029/2009GL042196.
Shuman, B.N., Carter, G.E., Hougardy, D.D., Powers, K., Shinker, J.J., 2014. A north–south moisture dipole at multi-century scales in the Central and Southern Rocky Mountains, U.S.A., during the late Holocene. Rocky Mt. Geol. 49, 33–49. https://doi.org/10.2113/gsrocky.49.1.33.
Stansell, N.D., Abbott, M.B., Rull, V., Rodbell, D.T., Bezada, M., Montoya, E., 2010. Abrupt Younger Dryas cooling in the northern tropics recorded in lake sediments from the Venezuelan Andes. Earth Planet Sci. Lett. 293, 154–163. https://doi.org/10.1016/j.epsl.2010.02.040.
Stansell, N.D., Steinman, B.A., Abbott, M.B., Rubinov, M., Roman-Lacayo, M., 2013. Lacustrine stable isotope record of precipitation changes in Nicaragua during the Little Ice Age and Medieval Climate Anomaly. Geology 41, 151–154. https://

doi.org/10.1130/G33736.1.
Steinman, B.A., Abbott, M.B., 2013. Isotopic and hydrologic responses of small, closed lakes to climate variability: Hydroclimate reconstructions from lake sediment oxygen isotope records and mass balance models. Geochem. Cosmochim. Acta 105, 342–359. https://doi.org/10.1016/j.gca.2012.11.027.
Steinman, B.A., Abbott, M.B., Mann, M.E., Ortiz, J.D., Feng, S., Pompeani, D.P., Stansell, N.D., Anderson, L., Finney, B.P., Bird, B.W., 2014. Ocean-atmosphere forcing of centennial hydroclimate variability in the Pacific Northwest. Geophys. Res. Lett. 41 https://doi.org/10.1002/2014GL059499.
Steinman, B.A., Abbott, M.B., Mann, M.E., Stansell, N.D., Finney, B.P., 2012. 1,500 year quantitative reconstruction of winter precipitation in the Pacific Northwest. Proc. Natl. Acad. Sci. U. S. A 109. https://doi.org/10.1073/pnas.1201083109.
Steinman, B.A., Abbott, M.B., Nelson, D.B., Stansell, N.D., Finney, B.P., Bain, D.J., Rosenmeier, M.F., 2013. Isotopic and hydrologic responses of small, closed lakes to climate variability: Comparison of measured and modeled lake level and sediment core oxygen isotope records. Geochem. Cosmochim. Acta 105, 455–471. https://doi.org/10.1016/j.gca.2012.11.026.
Steinman, B.A., Pompeani, D.P., Abbott, M.B., Ortiz, J.D., Stansell, N.D., Finkenbinder, M.S., Mihindukulasooriya, L.N., Hillman, A.L., 2016. Oxygen isotope records of Holocene climate variability in the Pacific Northwest. Quat. Sci. Rev. 142, 40–60. https://doi.org/10.1016/j.quascirev.2016.04.012.
Steinman, B.A., Rosenmeier, M.F., Abbott, M.B., 2010a. The isotopic and hydrologic response of small, closed-basin lakes to climate forcing from predictive models: Simulations of stochastic and mean state precipitation variations. Limnol. Oceanogr. 55, 2246–2261. https://doi.org/10.4319/lo.2010.55.6.2246.
Steinman, B.A., Rosenmeier, M.F., Abbott, M.B., Bain, D.J., 2010b. The isotopic and hydrologic response of small, closed-basin lakes to climate forcing from predictive models: Application to paleoclimate studies in the upper Columbia River Basin. Limnol. Oceanogr. 55, 2231–2245. https://doi.org/10.4319/lo.2010.55.6.2231.
Stewart, I.T., Cayan, D.R., Dettinger, M.D., Stewart, I.T., Cayan, D.R., Dettinger, M.D., 2005. Changes toward Earlier Streamflow Timing across Western North America. J. Clim. 18, 1136–1155. https://doi.org/10.1175/JCLI3321.1.
Stone, J.R., Fritz, S.C., 2006. Multidecadal drought and Holocene climate instability in the Rocky Mountains. Geology 34, 409–412. https://doi.org/10.1130/G22225.1.
Stott, L., Timmermann, A., Thunell, R., 2007. Southern Hemisphere and deep-sea warming led deglacial atmospheric CO2 rise and tropical warming. Science 318, 435–438. https://doi.org/10.1126/science.1143791.
Sun, W., Jayaraman, S., Chen, W., Persson, K.A., Ceder, G., 2015. Nucleation of metastable aragonite CaCO3 in seawater. Proc. Natl. Acad. Sci. U. S. A 112, 3199–3204. https://doi.org/10.1073/pnas.1423898112.
Talbot, M.R., 1990. A review of the palaeohydrological interpretation of carbon and oxygen isotopic ratios in primary lacustrine carbonates. Chem. Geol. Isot. Geosci. Sect. 80, 261–279. https://doi.org/10.1016/0168-9622(90)90009-2.
Talbot, M.R., Johannessen, T., 1992. A high resolution palaeoclimatic record for the last 27,500 years in tropical West Africa from the carbon and nitrogen isotopic composition of lacustrine organic matter. Earth Planet Sci. Lett. 110, 23–37. https://doi.org/10.1016/0012-821X(92)90036-U.
Talbot, M.R., Kelts, K., 1990. Paleolimnological Signatures from Carbon and Oxygen Isotopic Ratios in Carbonates from Organic Carbon-Rich Lacustrine Sediments. In: Lacustrine Basin Exploration: Case Studies and Modern Analogs, pp. 99–112.
Telford, R.J., Barker, P., Metcalfe, S., Newton, A., 2004. Lacustrine responses to tephra deposition: Examples from Mexico. Quat. Sci. Rev. https://doi.org/10.1016/j.quascirev.2004.03.014.
Thompson, R.S., Whitlock, C., Bartlein, P.J., Harrison, S.P., Spaulding, W.J., 1993. Climatic changes in the western United States since 18,000 yr B.P. In: Wright Jr., H.E., Kutzbach, J.E., Webb III, T., Ruddiman, W.F., Street-Perrott, F.A., Bartlein, P.J. (Eds.), Global Climates since the Last Glacial Maximum. University of Minnesota Press, Minneapolis, pp. 468–512.
USDA, NRCS, 2017. Web Soil Survey.
Vacco, D.A., Clark, P.U., Mix, A.C., Cheng, H., Edwards, R.L., 2005. A speleothem record of Younger Dryas cooling, Klamath Mountains, Oregon, USA. Quat. Res. 64, 249–256. https://doi.org/10.1016/j.yqres.2005.06.008.
Valero-Garcés, B.L., Kelts, K.R., 1995. A sedimentary facies model for perennial and meromictic saline lakes: Holocene Medicine Lake Basin, South Dakota, USA. J. Paleolimnol. 14, 123–149. https://doi.org/10.1007/BF00735478.
Valero-Garcés, B.L., Laird, K.R., Fritz, S.C., Kelts, K., Ito, E., Grimm, E.C., 1997. Holocene Climate in the Northern Great Plains Inferred from Sediment Stratigraphy, Stable Isotopes, Carbonate Geochemistry, Diatoms, and Pollen at Moon Lake, North Dakota. Quat. Res. 48, 359–369. https://doi.org/10.1006/qres.1997.1930.
Waitt, R.B., Thorson, R.M., 1983. The Cordilleran Ice Sheet in Washington, Idaho and Montana. In: Late-quaternary Environments of the United States, pp. 53–70.
Whitlock, C., 1992. Vegetational and climatic history of the Pacific Northwest during the last 20,000 years: implications for understanding present-day biodiversity. Northwest Environ. J. 8, 5–28.
Whitlock, C., Brunelle, A., 2006. Pollen records from northwestern North America. In: Elias, S. (Ed.), Encyclopedia of Quaternary Science. Elsevier, Amsterdam, pp. 1170–1178.
Whitlock, C., Dean, W.E., Fritz, S.C., Stevens, L.R., Stone, J.R., Power, M.J., Rosenbaum, J.R., Pierce, K.L., Bracht-Flyr, B.B., 2012. Holocene seasonal variability inferred from multiple proxy records from Crevice Lake, Yellowstone National Park, USA. Palaeogeogr. Palaeoclimatol. Palaeoecol. 331–332, 90–103. https://doi.org/10.1016/j.palaeo.2012.03.001.
Wright, H.E., Mann, D.H., Glaser, P.H., Ybert, J.-P., Engstrom, D.R., Cole-Dai, J., Bolzan, J.F., Liu, K. -b., 1984. Piston Corers for Peat and Lake Sediments. Ecology 65, 657–659. https://doi.org/10.2307/1941430.
Zdanowicz, C.M., Zielinski, G.A., Germani, M.S., 1999. Mount Mazama eruption: Calendrical age verified and atmospheric impact assessed. Geology 27, 621–624. https://doi.org/10.1130/0091-7613(1999)027<0621:MMECAV>2.3.CO;2.
Zobel, D.B., Antos, J.A., 1997. A decade of recovery of understory vegetation buried by volcanic tephra from Mount St. Helens. Ecol. Monograph 67, 317–344. https://doi.org/10.1890/0012-9615(1997)067[0317:ADOROU]2.0.CO;2.